Geochemical News 144 - September 2010

In This Issue

GNews 144 Staff

Stephen Komor, Ph.D. (Editor)
U.S. Geological Survey (retired)
sck15@cornell.edu

Seth Davis (Webmaster)
Geochemical Society
seth.davis@geochemsoc.org

Share your views on future research directions in the Earth sciences

To all members of the Geochemical Society:

Your input is needed for an important study being conducted by the National Research Council's Committee on New Research Opportunities in the Earth Sciences. The committee is charged with

> (1) identifying high-priority new and emerging research opportunities in the Earth sciences over the next decade, including surface and deep Earth processes and interdisciplinary research within fields such as ocean and atmospheric sciences, biology, engineering, computer science, and social and behavioral sciences, and
>
> (2) identifying key instrumentation and facilities needed to support these new and emerging research opportunities.

The committee would like your perspective regarding future research in the Earth sciences. Please take a few minutes to respond to the three questions at the following link:

> http://thenationalacad.nroes.sgizmo.com

The report will have the biggest impact if each community is well represented. This is your opportunity to share your views with NSF and the broader Earth science community.

Thank you for taking the time to participate in this important survey.

Timothy W. Lyons
Department of Earth Sciences
University of California

A Historical Perspective of the Development of the CheMin Mineralogical Instrument for the Mars Science Laboratory Mission

by David Blake, NASA Ames Research Center

David Blake

Introduction by Paul Mahaffy (NASA Goddard Space Flight Center)
Volumes of multispectral infrared imaging data presently flowing in from Mars orbiting spacecraft are giving us a new view of the planet (Ehlman, Geochemical News 142) and pointing toward candidate landing sites for surface rovers. Highly ruggedized and miniaturized instruments on future rovers will carry out an even more detailed exploration of the chemistry and mineralogy at the most interesting sites to elucidate geological and geochemical processes that may point toward habitable environments for past or present life. One such instrument planned for use on the Curiosity rover that is planned to land on Mars in 2012 is the x-ray fluorescence/x-ray diffraction instrument CheMin described in this contribution from the Principle Investigator for this investigation, David Blake. Some of the robust field-testing of this instrument on remote Mars analog sites in the Arctic Svalbard archipelago is also described.

In our solar system, Mercury, Venus, Earth and Mars are rocky planets; Jupiter, Saturn, Uranus and Neptune are gas giants with no solid surfaces, and Pluto (now, sadly, demoted to 'planetesimal' status) is icy and cryogenically cold. Early in Solar System history, surface conditions on Mars and Venus diverged from what could have been a 'habitable' status. Venus is not presently habitable due to its high surface temperature and inhospitable atmospheric composition. Furthermore, present day surface temperatures and atmospheric conditions on Venus would have likely destroyed any evidence of earlier habitable conditions. Mars cooled off and lost most of its atmosphere, but still preserves geological evidence of its early history - a time when its climate was much more clement than the present day. With the exception of 'special' zones such as the proposed subsurface ocean of Jupiter's moon Europa or the organic-rich surface of Saturn's moon Titan, 'habitable zones' are more or less confined to the surface and near-surface environments of Earth and Mars. For the foreseeable future then, Mars seems to be the most promising place in the solar system to look for evidence of past or present extraterrestrial life.

An important difference between Mars and Earth is the apparent absence of extensive plate tectonics on Mars. On Earth, as a result of plate tectonic movements, most surface crustal components older than ~3 billion years have been subsumed by convergent plate margins or metamorphosed beyond recognition of origin or both. Truly ancient crust that existed in the habitable zone when early terrestrial life developed and radiated can only be found in highly deformed slivers of rocks in a few places in the world. By contrast, much of the Mars surface from that early epoch has been preserved relatively unaltered. Thus, there is the possibility on Mars to study relatively unaltered crust in which habitable zones were preserved at the time when terrestrial life originated and radiated.

Our recent knowledge of early geology and potentially habitable environments on Mars is derived from decades of study of Mars meteorites such as ALH 84001, from the orbital observations of Mars Observer, Mars Reconnaissance Orbiter and the European Space Agency's Mars Express Orbiter, from Mars Pathfinder and from the Mars Exploration Rovers. We hope to continue the rich heritage of Mars science during the upcoming Mars Science Laboratory Mission.

The Mars Science Laboratory Mission

Mars Science Laboratory (MSL '11) is NASA's follow-on landed mission to the Mars Exploration Rovers Spirit and Opportunity, which, more than 6 years after their intended 90-day lifetimes, are still making fundamental scientific discoveries on the Mars surface. MSL is intended to '…Explore and quantitatively assess a local region on the Mars surface as a potential habitat for life, past or present.' The duration of the primary mission of MSL will be 670 sols, or one Mars year (about two Earth years). During this time, the plan is for the MSL rover (named 'Curiosity') to traverse to at least 3 geologically distinct sites within its 20 km diameter landing ellipse and determine the 'habitability' of these sites (habitability is defined in this context as the 'capacity of the environment, past or present, to sustain life').

The CheMin instrument will be principally engaged in the following MSL science objectives:

- Characterizing the geology and geochemistry of the landed region;
- Investigating the chemical and mineralogical composition of Martian surface and near-surface geological materials;
- Interpreting the processes that have formed and modified rocks and regolith.

MSL carries four types of instruments: 'Environmental instruments' such as the Radiation Assessment Detector ('RAD') and the Rover Environmental Monitoring Station ('REMS'), 'remote observation' instruments such as the Mast Camera ('Mastcam'), the Mars Descent Imager ('MARDI') the Chemistry-and-Camera ('ChemCam') and the Dynamic Albedo of Neutrons ('DAN'), and 'arm instruments' including the Alpha Particle X-ray Spectrometer ('APXS') and the Mars Hand Lens Imager ('MAHLI'). Inside the body of the rover is the 'Analytical Laboratory' which is comprised of the Chemistry and Mineralogy ('CheMin') instrument and the Sample Analysis at Mars ('SAM') instrument suite. Each of these instruments, as well as the mission itself, is described in detail on the MSL mission website.[1]

Together, the environmental, remote and arm instruments of *Curiosity* operate much like a field geologist would on Earth - identifying interesting rocks or formations from a distance (even obtaining an elemental analysis from up to 10 meters using ChemCam), then approaching them to make *in situ* hand lens observations and elemental analyses. These operations and observations are similar to those performed by *Spirit* and *Opportunity* for the past 6 years. However, once these operations are performed, *Curiosity* goes further. *Curiosity* can collect, prepare and analyze samples in much the same way that this is done in a terrestrial laboratory. When a sample is found to be interesting by scientists on Earth, *Curiosity* will deploy an arm-mounted percussion drill called 'PADS' (Powder Acquisition Drill System) in concert with a sample processing system called 'CHIMRA' (Collection and Handling for Interior Martian Rock Analysis) to collect material for further analysis. Drilled or scooped material is then sieved and a portion of this sieved material is transferred to the Analytical Laboratory. *Curiosity's* Analytical Laboratory can conduct quantitative mineralogical analysis (CheMin) and organic and isotopic analysis (SAM) of material delivered through funnels into the body of the rover. Once a complete analysis is obtained by the Analytical Laboratory, results are sent back to Earth for interpretation

About the Author

David F. Blake is co-investigator of Photosynthetic and Chemosynthetic Ecosystems for NASA's Space Science and Astrobiology at Ames.

obtained by the Analytical Laboratory, results are sent back to Earth for interpretation.

How does CheMin work?

CheMin determines the mineralogy of crushed or powdered samples through X-ray diffraction (XRD) and elemental composition through X-ray Fluorescence (XRF). XRD is an extraordinarily powerful technique that identifies the structures of crystalline materials from first principles, and is the preferred method for mineralogical analysis in terrestrial laboratories.

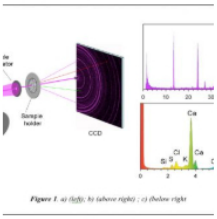

Figure 1

During a mineralogical analysis, a ~50 µm collimated X-ray beam from an X-ray tube source is directed through powdered or crushed sample material. An X-ray sensitive CCD imager on the opposite side of the sample from the source directly detects X-rays diffracted or fluoresced by the sample (Figure 1a) < Details of the CCD operation are shown in Apendix A>.

During an X-ray Diffraction analysis, CheMin's CCD detector is exposed to the X-ray flux, read out and erased many times (100-1000 exposures). The detected X-rays are used to produce both diffraction and fluorescence data. Diffracted primary beam X-rays strike the detector and are identified by their energy. A two-dimensional image of these X-rays constitutes the diffraction pattern (Fig. 1a). At incremental radii this pattern is summed circumferentially about the central undiffracted beam to yield a 1- dimensional 2θ plot comparable to conventional diffractometer data (Fig. 1b). All of the X-rays detected by the CCD are summed into a histogram of number of photons vs. photon energy that constitutes an XRF analysis of the sample (Fig. 1c).

The requirement for CheMin to perform X-ray Fluorescence (XRF) elemental analysis was removed early in the spacecraft instrument design phase. The energy-dispersive X-ray histograms obtained during an analysis will only be used to construct energy-selected diffraction patterns, such as CoKα. When this is done, sample fluorescence, multiple photon detections in a single pixel, tracks from cosmic rays, etc. can be removed from the patterns. While the requirement to perform XRF elemental analyses was descoped by the MSL project, these data are still obtained by the instrument and will be analyzed on a 'best effort' basis.

Quantitative mineralogical results are obtained from XRD data by Rietveld refinement and other full-pattern fitting techniques. 2,3 Both crystalline and amorphous materials can be analyzed in this way. The duration of a single XRD experiment sufficient to quantitatively analyze a single mineral such as quartz or olivine, is less than one hour and consumes a few tens of Watts. Complex assemblages such as basalts having 4 or more minerals plus glass may require the summation of 4-8 of these experiments over 1 or more Mars sols.

Prototypes and Terrestrial Analogs of the CheMin Instrument

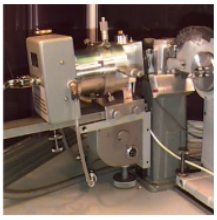

Figure 2a

During the development of the CheMin instrument concept, several prototypes were built which had increasing fidelity to what would become the flight instrument. The CheMin I instrument consisted of a commercial CCD camera in an evacuated housing with rudimentary sample handling mechanisms, interfaced to a commercial X-ray tube tower (Fig. 2a). An evacuated housing was necessary because the CCD was cooled to -60 C during operation. The electronics and power supplies for this machine - and the X-ray source - occupied a small room. CheMin II was an improvement relative to CheMin I in that a self-contained X-ray tube and power supply was interfaced to a sealed and evacuated commercial CCD camera (Fig. 2b). A thin beryllium window allowed X-rays to enter the camera and expose the CCD. Because the samples were analyzed in room air, we could experiment more freely with sample types and sample delivery / sample movement mechanisms.

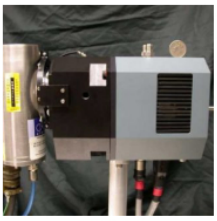

Figure 2b

A breakthrough in sample handling occurred between CheMin II and III. For a sample to be optimally prepared for powder XRD, it must be ground to somewhat less than 10 µm particle size, a difficult task even in terrestrial laboratories (this is basically the same grain size as flour or face powder). The reason for this is that in order to get a pattern with all diffraction peaks present at their correct intensities, random orientations of myriads of tiny crystallites are required. We had experimented with finely ground pressed powders translated with an x,y stage, but nothing seemed to work particularly well. CheMin Co-I Philippe Sarrazin proposed a sample holder in which loose powder is held between two X-ray transparent plastic windows spaced ~200 µms apart. By vibrating the sample holder at sonic frequencies with a piezoelectric device, (we first used modified buzzers from Radio Shack) the powder was made to flow like a liquid inside the cell. This solved our two most difficult sample handling problems - exposing a representative amount of the sample to the 50 µm diameter X-ray beam during the analysis, and rotating the grains to all orientations as they passed through the beam. We found that powders ground and sieved to less than 150 µm diameter produced excellent patterns. Rock powder produced by a variety of techniques (drilling, grinding, crushing) has a significant fraction in this size range and below.

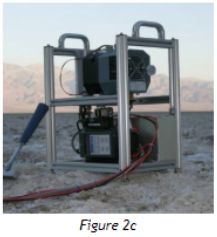

Figure 2c

CheMin III was our first field demonstration model, and consisted of the basic components of CheMin (X-ray tube, Sample handling system and CCD camera) held in a portable frame along with control electronics and power supplies (Fig. 2c). The instrument was powered through a cable connected to several motorcycle batteries, and operated through a laptop computer. CheMin III was demonstrated in Death Valley, CA in 2003. However, the entire system still occupied the trunk of a car and had limited durability at remote localities. CheMin IV was the first truly portable CheMin system. While it appears much like the earlier model, it was operated by an integrated microcomputer and powered by on-board Li-ion batteries and a power management system. Data were transferred to a laptop computer using a USB thumb drive, and processed off-line. CheMin IV was used to obtain the first remote quantitative mineralogical analysis by David Bish of Indiana University during a field expedition to Svalbard, Norway, in 2006 (Fig. 2d).

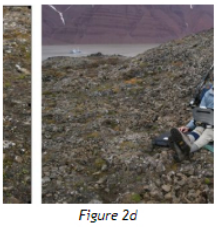

Figure 2d

The CheMin Flight Instrument

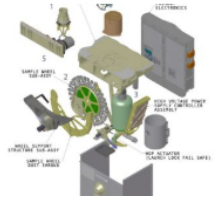

Building a successful flight instrument is a task that is breathtakingly hard, and best left to professionals. MSL instruments are required to operate for a full Martian year on the Mars surface, in temperatures that vary from -70 C to +50 C (instruments outside the body of the rover are required to survive temperatures as low as -130 C). They must survive intense vibration during launch, transit to Mars in vacuum and ultimately operate under varying thermal and atmospheric conditions, as well as survive the intense neutron flux from the DAN instrument and from Curiosity's Radioisotope Thermoelectric Generator (RTG). Every fastener and component is tested under the full range of conditions and spares of

Figure 3

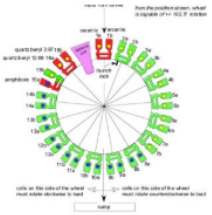

Figure 4

critical components are 'life-tested' for 1.5 times the nominal mission duration. The CheMin flight instrument (also called the 'Flight Model,' or 'FM') was built by scientists, engineers and technicians at NASA's Jet Propulsion Laboratory during 2005-2009, and delivered to the MSL project in June, 2010. A CheMin 'Demonstration Model', or 'DM' is also being constructed that is an exact copy of the FM, and will be used for testing Mars analog samples, as well as for studying potential instrument anomalies during the MSL mission. '

An exploded view of the spacecraft instrument is shown in Fig 3. The CheMin sample handling system consists of a funnel, a sample wheel (which carries 27 reusable sample cells and 5 permanent reference standards), and a sample sump where material is dumped after analysis (Fig. 4). CheMin receives sieved drill powders or scoop samples from PADS/CHIMRA (*Details of sample delivery and processing are described in Appendix B*).

A full analysis of an individual sample is called a 'major frame' and will require as many as 10 hours of analysis time, accumulated over multiple sols. Once a major frame of data is sent to ground and accepted, the analyzed material is emptied from the cell and that cell is ready to be reused. CheMin does not have the capability to store previously analyzed samples for later re-analysis (*Details of CheMin sample handling and analysis are described in Appendix C*).

X-ray Diffraction Mode

The CCD is placed in the forward-scattered direction relative to the X-ray beam so that mineral phases with large interplanar spacings (and hence narrow diffraction cones at low 2θ), such as clays, can be detected. In addition, low-index lines (which are commonly the most intense and most definitive for phase identification) occur in the forward-scattered direction. Table 1 shows the expected 2θ range (for Co Kα radiation) and 2θ Full Width at Half-Maximum (FWHM) for X-ray diffraction.

A special case of X-ray detection by the CCD is the detection of Co Kα characteristic photons from the primary source. When Co Kα photons are detected, the X,Y pixel location on the CCD is identified and the corresponding X,Y location in a 600x582 counting number array is incremented by one. This process results in a Co Kα diffraction image. Various strategies are used in on-board data processing to optimize the quality or quantity of diffraction data returned (e.g., 'single pixel' detection, and 'split pixel' detection, etc.

An additional 600x582 array stores an image of all of the photons detected by the CCD regardless of energy. This array acts very much like a piece of photographic film, recording the Co Kα XRD pattern as well as background, X-ray Fluorescence from the sample, and Bremsstrahlung radiation from the X-ray source.

XRD/XRF Calibration and Characterization

Five permanent cells are loaded with calibration standards (Fig. 4). Three of these cells are loaded with single minerals or a synthetic ceramic and two are loaded with differing quartz/beryl mixtures. Basic calibration, completed prior to delivery of the instrument to MSL Assembly, Test, and Launch Operations (ATLO), was performed using only the five permanent standards loaded into the sample cells of the FM.

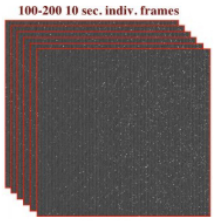

Figure 6a

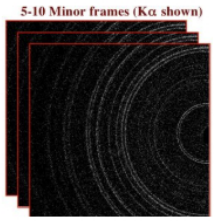

Figure 6b

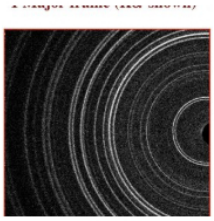

Figure 6c

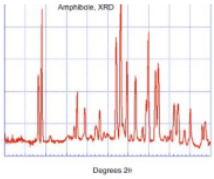

Kα XRD

Figure 6d

Calibration of these standards entails measurement of 2θ range and 2θ FWHM for XRD, and of the required XRF energy range and FWHM for elemental peaks, in particular Fe Kα, Co Kα and Co Kβ. Quantitative accuracy, precision and detection limits are evaluated using the quartz-beryl standards (CheMin's requirements for detection limit, accuracy and precision of analyses are shown in Table 2). Figures 6-7 show data from Cryo-Vac tests of the flight instrument. Fig. 6a-c show single frame, minor frame and major frame data from the amphibole standard. Fig. 6d shows an energy dispersive X-ray histogram for a single frame, and Fig. 6e shows the energy dispersive X-ray histogram for all of the single frames summed into the major frame. Figure 6f shows a 1-D diffractogram obtained for a major frame (full analysis) of the amphibole. Figure 7 illustrates the 'best case' X-ray Fluorescence capability of the instrument. These data were obtained by analyzing the synthetic ceramic standard, prepared to evaluate the XRF capability of the instrument.

Quantitative XRD calibration of the Development Model (DM) and other CheMin Testbeds

Quantitative XRD (QXRD) calibration will be performed using the DM and various other testbeds. For QXRD calibration, synthetic mixtures that mimic real samples likely to be encountered on Mars have been prepared from minerals mixed in known weight fractions, or natural materials of known composition.

For characterization of CheMin operation across a broad spectrum of samples, synthetic and natural, the DM will be supported by testbeds and facilities that replicate various parts of the DM/FM function with varying levels of fidelity:

The Development Model: The DM will be set up in a testbed configuration at JPL in CheMin Co-I Albert Yen's laboratory. Prior to launch, the DM will be used to test algorithms, establish calibrations, develop operation scenarios, and characterize Mars analog samples. During landed operations the DM unit will be used to test new command sequences, develop operational scenarios, characterize Mars analog samples and reproduce any instrument anomalies that might occur during the MSL mission.

Analytical facility for Mars analog rocks: The Planetary Mineralogy and Spectroscopy Laboratory at NASA Ames Research Center (ARC) will house several CheMin analog instruments. The principal instruments in this laboratory are a CheMin IV instrument4 and a Terra instrument5 (a field-deployable instrument based on the CheMin design that was developed by InXitu, Inc). These instruments will be used to analyze Mars analog rocks in a geometry similar to the CheMin FM and the DM instruments. A commercial InelTM X-ray diffractometer at Ames Research Center is configured to analyze Mars analog rocks in a geometry nearly identical to the CheMin flight instrument. This instrument is equipped with a Co X-ray tube and a 120-degree parallel detection system capable of collecting XRD patterns with a higher 2θ resolution than the spacecraft instrument (but which can be degraded to MSL CheMin resolution for comparison and pattern matching). A Mars atmospheric pressure chamber is installed with a carousel and MSL funnel, and a CheMin transmission sample cell capable of being filled, piezo-electrically shaken during analysis and dumped. A large number of patterns of Mars analog rocks and soil are being collected for analysis prior to, during and after the prime MSL mission. The CheMin IV and Terra instruments have

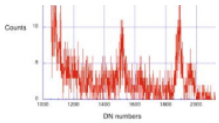

Single frame histogram

Figure 6e

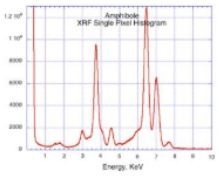

XRF spectrum

Figure 6f

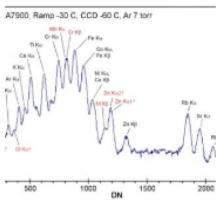

Figure 7

the resolution and diffraction geometry of the MSL Flight instrument and will be used in supporting tests.

CheMin Instrument Modes

During a nominal 10-hour analysis, CheMin collects and stores X-ray data as individual 600x582 pixel CCD images of 5-30 seconds exposure each. A 'minor frame' consists of 30 minutes of these images, nominally 360-60 frames depending on integration time. A complete 10-hour analysis of a sample comprises 20 such minor frames and is called a 'major frame.'

There is insufficient bandwidth to deliver all of CheMin's raw data to Earth. When commanded, CheMin will deliver raw data to the Rover Compute Element (RCE) that in turn partially processes the raw data for each minor frame, in order to reduce the data volume. Each minor frame of data transmitted to Earth contains one or more raw frames in order to assess the health of the detector, a variety of engineering and health information about the instrument, and one or more of three possible processed data products. The three types of data products are described below:

- 'Fully processed mode': Each image is reduced to a pixel map containing ones and zeros, where '1' represents the detection of a photon within a specific energy window (e.g., Co Kα), and '0' represents everything else. Each pixel map is summed into a 600x582 counting number array of pixel positions; the result is a 2-D energy-filtered diffraction pattern. In addition to the energy-filtered diffraction pattern, 'fully processed mode' also provides a histogram of all of the photons detected vs. energy, which amounts to an X-ray energy-dispersive spectrum of the sample material.
- 'Film mode': Each image is summed into a 600x582 array as raw data. A single real number array holds the summed image for each minor frame.
- 'Modified raw mode': Pixels below a selected threshold are set to zero, and pixels that are above that threshold are run-length encoded with x, y, and intensity information preserved.

Analysis of diffraction data in the tactical time frame: Immediately after a downlink of CheMin data, the downlink lead will process the minor frames to create 1-D 2θ plots. These 1-D plots or 'diffractograms' will be analyzed and compared with the ICDD (International Centre for Diffraction Data) PDF-2 powder diffraction file and the AMCSD (American Mineralogist Crystal Structure Database) to determine major mineral components. CheMin Science Team members will offer preliminary identifications of any major or clearly discernable mineral components during this tactical cycle. Periodically these data will support a 'drive away' or 'stay' decision for rover operations.

Analysis and refinement of diffraction data in the strategic time frame. Rietveld computational refinement methods and full pattern fitting, among others, will be utilized to perform a quantitative analysis of each pattern. These patterns will be compared with library patterns to identify mineral components and to derive quantitative mineral abundances. Analyses will be updated on a continuous basis as insights are made as to the identity of major and minor phases, and X-ray amorphous materials.

Mars on Earth - Utilization of CheMin Prototype Instruments during the AMASE (Arctic Mars Analog Svalbard Expeditions) to Svalblard, Norway

Figure 8

The first deployment of CheMin IV to Svalbard was thought provoking for us, because while we had approached it principally as a technology demonstration, we discovered quickly that in situ mineralogical analyses were actually useful for the geologists conducting fieldwork. The change from the usual procedure of first conducting field work and later performing laboratory mineralogical analysis suffers for the fact that hypotheses generated in the field can typically only be evaluated after the geologists have left the field area. Geologists commonly collect a comprehensive set of samples from the field and make the assumption that the mineralogical information necessary to support or modify an already formed hypothesis is in hand. With in situ mineralogical analyses, field geologists are able to test hypotheses while in the field, and alter their collection/analysis strategy (or even modify their working hypotheses) based on the field data. However, in order for CheMin IV to be truly useful, user-friendliness, portability and pattern acquisition speed had to be improved. The next generation system was called mini-CheMin, and was made smaller and more portable, and contained all the hardware and software necessary to provide diffractograms as data were collected (Fig. 8). Diffraction data are transmitted wirelessly to a laptop system and analyzed using commercial programs like MDITM Jade or XpowderTM. MiniCheMin proved to be highly useful, and a commercial version called 'Terra' is now offered by a company called inXitu, Inc. With increased tube power and optimized geometry, XRD patterns of complex mineralogies can be acquired in 5-15 minutes, and single minerals such as quartz can be identified in as little as 20 seconds. With the increase in data collection speed, field-deployed XRD is now possible on the same time scale as other field-portable techniques such as XRF Spectrometry, laser-Raman and IR imaging. The advantage of XRD over these other techniques is that it is a true phase identification technique, and it is possible to quantify mineralogical results.

When a rover is deployed on Mars, time is money. If one divides the full cost of a Mars rover by the number of sols (days) in its active mission, the result is typically millions of dollars per sol. Decisions to move the rover, collect a sample or deploy one instrument vs. another are made on a time-critical, tactical basis. Because data are relayed to an orbiting Mars satellite only when the rover is in sight of the orbiter, then downlinked to the Deep Space Network (DSN) on Earth only when the orbiter is in sight of Earth, just a few hours are available for the Science Operations Working Group (SOWG) to analyze the data before the next command sequence has to be uplinked to the rover. During this time, the SOWG must converge on an interpretation of the downlinked data, come to a consensus as to the next day's operations, then code and relay those instructions through the DSN to the Mars orbiting satellite and down to the rover. Each day's activities are proscribed by the total energy and time made available to the instrument suite, the energy and time required for data acquisition for each individual instrument, the priority of desired measurements, and the total data volume that can be transmitted back to Earth. All of this means that instrument deployment and data interpretation, as well as the sequence in which particular measurements are made, require a thorough knowledge of instrumental capabilities, limitations and instrument synergisms one to another.

Many instrument providers have not had prior experience in instrument operations on Mars (the author included). So that potential instrument providers can become proficient in these activities, NASA initiated a program called the Astrobiology Science and Technology for Exploring Planets (ASTEP). Typically, ASTEP deployments involve instrument operations in remote areas of Earth, on Mars-like (or other extraterrestrial) terrains. Two types of activities are conducted: In one type of activity, a scientific theme is pursued that has relevance to future missions: Habitability, Life Detection or Sample Return among them. A variety of instruments is utilized in the field to collect data useful in solving the multidisciplinary science or engineering problem that is posed. In a second type of activity, called a 'Fast-Motion' field test ('FMFT'), a suite of Mars analog instruments is deployed in the field by one group of scientists ('the rover team') while a second group of scientists (the Science Operations Working Group, or 'SOWG') is sequestered away from the field area. The SOWG learns about the field area by

deploying 'rover instruments' and analyzing data returned by the rover team under the same constraints that are faced by a SOWG during a real Mars mission (except that several Mars sols of activity can be completed in a single day).

Figure 9

Svalbard, Norway is an ideal location for ASTEP instrument deployments. At nearly 80° North latitude, the archipelago is almost devoid of plants larger than mosses, and mountain glaciers have created deeply scoured valleys, effectively the world's largest 'road cuts' (Fig. 9). Rock exposures are breathtaking, and the lack of human habitation (with the exception of a few isolated towns) has left much of the landscape pristine. Svalbard has official status as an International Science Preserve, managed by the Norwegian government.

Initial interest in Svalbard for NASA research activities was engendered by the petrologic field work of Hans Amundsen (then at the University of Oslo).6 In 1997-1999, in the midst of the flurry of research activities associated with characterizing the ALH84001 meteorite (which was purported to have evidence of life7), Amundsen collaborated with Allan Treiman of the Lunar and Planetary Institute and the author (Ames Research Center) to characterize carbonate globules similar to those described from ALH84001, found in ultramafic xenoliths from Svalbard.8 Now in its 7th year, AMASE conducts yearly expeditions to Svalbard, providing a base of operations for scientists and technologists from many countries. Both NASA and ESA (European Space Agency) use AMASE as a testing ground for flight instrument prototypes and for conducting interdisciplinary science similar to that which occurs during landed planetary missions.

There is a variety of sedimentary, metamorphic and volcanic terrains in Svalbard.9 CheMin prototype instruments such as Terra have principally been deployed in volcanic areas, analyzing basalts, volcanic soils,10 ultramafic xenoliths and their weathering products11 and secondary Fe-Mg carbonates associated with late-stage hydrothermal events.12 Hydrothermal activity associated with volcanism was probably common on early Mars, which featured abundant basaltic rocks, water as ice or liquid, and heat from volcanoes and asteroid impacts. The most primitive forms of life on Earth still prefer hydrothermal environments, and such environments - and their habitability - can be studied either as presently active systems, or as fossil systems in the geologically near-recent of Svalbard. Early organisms were probably chemolithotrophic (they derived their energy from inorganic reactions in rocks), and a second possible habitable zone for early chemolithotrophic organisms in Svalbard is created by the weathering of ultramafic minerals such as olivine to form serpentine with the release of hydrogen.13

Figure 10

The style of volcanism in Svalbard is unique, in that the eruptive activity apparently occurred under ice, and the source magmas were volatile rich. Ultramafic xenoliths comprise as much as 20% of the volume of eruptive material, suggesting a deep source for the magma. Several Quaternary volcanic centers are prominent in the field areas studied by AMASE. Sverrefjell is a stratovolcano or large cinder cone ~500 m tall on the shore of Bokfjord (Fig. 9). Horizons of pillow lavas, indicative of eruption in water or under ice, exist nearly to the top of the volcano, and glacial erratics can be found at Sverrefjell's summit, indicating that the volcano was covered with thick ice either during or soon after its eruption. The style of eruption of Siggurdfjell is less obvious but probably was a volcanic neck or fissure, exposed up to 1000 m above present sea level. Fe-Mg carbonates are found in a variety of petrologic rock types and regimes on both Sverrefjell and Siggurdfjell. Ultramafic xenoliths, abundant at both localities, contain carbonate globules nearly identical to those found in ALH84001.8 Several styles of volcanic vents, 1-10 m in width (Fig. 10) contain films, rinds or thick crusts of carbonate material, clearly precipitated from water in localized hydrothermal systems during the waning stages of eruptive activity. The Terra instrument was used for in situ analysis of these carbonates both at the sites of deposition, and aboard the Research Vessel Lance (our field station) directly after collection. These on-site mineralogical analyses allowed the formulation of hypotheses and collection/analysis strategies while scientists were still in the field, and also were used to direct the collection of samples used for other purposes, such as life marker chip, IR, laser Raman, Laser-Induced Breakdown Spectroscopy (LIBS) and Gas Chromatography-Mass Spectrometry (GC-MS).14

The value of Svalbard as a Mars analog site was recently proved out in a paper identifying carbonate-rich outcrops on Mars from data obtained during operations of the MER rover Spirit.15 In the paper, the authors reported finding carbonates with nearly identical composition to the ALH84001 meteorite and to those reported from Svalbard11 and concluded that the Martian carbonates were formed in basaltic hydrothermal systems, analogous to those described from Svalbard.

Less obvious but equally valuable are the personal bonds formed by the various interactions, arguments, compromises and group decisions made by geologists, biologists, chemists, physicists and engineers during many days of joint field activity and Fast Motion Field Tests. Interdisciplinary cooperation in the field between different scientific specialties, as well as between scientists of different nationalities, is also a hallmark of joint expeditions such as AMASE. As a result of the common interests of NASA and ESA, and the high cost of 'going it alone' when it comes to planetary exploration, a decision was recently reached by these agencies to work together on future Mars exploration. The collaboration, cooperation and respect engendered by joint research endeavors on Earth such as AMASE will pay dividends when the real missions come to fruition.

Future Versions of CheMin for Mars and Other Solar System Destinations

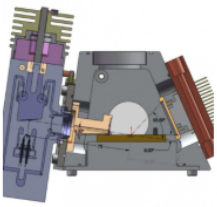

Figure 11a

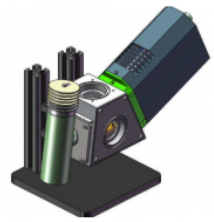

Figure 11b

A major drawback of CheMin XRD/XRF instruments developed to date is that samples must be prepared and delivered to the instrument as fine-grained powder. Two next-generation CheMin-like instruments funded for development by NASA are intended to minimize or overcome these sample handling problems. Luna (Fig. 11) is an XRD/XRF instrument intended for robotic missions to the Moon or any other airless body. Luna is a reflection mode instrument that will analyze soils without sample preparation. While there is still a requirement for fine-grained samples (as there is for all powder XRD instruments), the reflection geometry allows for less sophisticated sample delivery and sample handling systems. Due to the geometrical considerations of a compact reflection instrument, the low 2θ limit is 8° 2θ, too high for the detection of some clays. However, for almost all other minerals of geological interest, the lowest 2θ peaks of interest are not lower than 15° 2θ. A second Hybrid single crystal / powder XRD instrument is being designed and built as an arm instrument for small rovers (Fig. 12).16 No sample preparation will be necessary for this instrument, except perhaps for the creation of a flat surface much as the Rotary Abrasion Tool (RAT) creates on the Spirit and Opportunity rovers. As-received powders such as soils can be analyzed via powder XRD, much like Luna, but with multiple detectors (and multiple wavelengths of radiation). Rocks with mineral grain sizes larger than fine-grained powder (most crystalline rocks would fall into this category) would be analyzed using the single crystal Laue technique. This capability is made possible through the use of multiple energy-discriminating area detectors. Single crystal maxima can be identified by their energy and 3-dimensional position in space, and related back to the structure (and therefore identity) of the diffracting

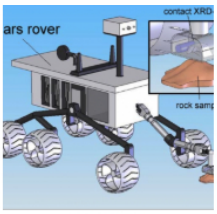

Figure 12a

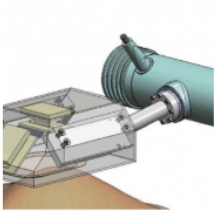
Figure 12b

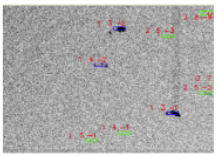
Figure 12c


Figure 13

mineral phase.

Spinoff CheMin Instruments for Terrestrial Use

Several instruments based on the CheMin design are now in commercial production. Terra is used as a CheMin analog instrument in NASA-sponsored field campaigns as well as a number of ESA and other field expeditions throughout the world. Terra is also used for mud-logging applications at oil drilling sites, in museums and at remote sites for analyzing geological materials for industrial processes.17

Pharmaceutical products are typically crystalline, and can be identified and quantified by XRD just as minerals are. The author is working with scientists from the Centers for Disease Control (CDC) and elsewhere to develop applications of Terra for the identification of counterfeit drugs in developing nations. First and foremost of these are the Malaria drugs. Nearly 1.5 million people, mostly children in developing nations, die of Malaria each year.18 Tens of thousands of these deaths are due to the scourge of counterfeit drugs, which in some places in SE Asia and equatorial Africa account for more than 50% of the drugs available.19 Simple and effective tests have been devised to detect the presence or absence of the active ingredient in malaria pills, artesunate. However, an increasing number of these counterfeit malaria drugs are being 'salted' with a small amount of artesunate to escape detection by these tests. This unfortunate practice is creating resistance in the malaria parasite for what is now the only drug that is effective in fighting the worst strains of the disease.20 Terra is quite good at quantifying artesunate in malaria pills and can do so in remote locations, at the source of the problem.21

CheMin-type instruments are also being used in the world of Art and Antiquities. A reflection XRD instrument called 'Duetto' was commissioned by Giacomo Chiari of the Getty Conservation Institute for characterizing art objects and intiquities.17,22 This instrument is now being used world-wide to characterize sensitive archeological artifacts, to evaluate the causes of deterioration of ancient murals and other artifacts in places such as Tutankhamen's tomb and the Roman ruins of Herculaneum, Italy (Fig. 13).

References

1. http://msl-scicorner.jpl.nasa.gov/Instruments/.
2. Bish, D.L. and J.E. Post (1993). 'Quantitative mineralogical analysis using the Rietveld full-pattern fitting method.' American Mineralogist 78, 932-942.
3. Chipera, S.J. and D.L. Bish (2002). 'FULLPAT: a full-pattern quantitative analysis program for X-ray powder diffraction using measured and calculated patterns.' J. Applied Crystallography 35, 744-749.
4. Bish, D.L., Blake, D., Sarrazin, P., Treiman, A.H., Hoehler, T., Hausrath, E.M., Midtkandal, I., and Steele, A. (2007). 'Field XRD/XRF mineral analysis by the MSL CheMin instrument.' LPSC XXXVIII, Abstract #1163.
5. Sarrazin, P., W. Brunner, D. Blake, M. Gailhanou, D.L. Bish, D. Vaniman, S. Chipera, D.W. Ming, A. Steele, I. Midtkandal, H.E.F. Amundsen and R. Peterson (2008). 'Field studies of Mars analog materials using a portable XRD/XRF instrument.' LPSC XXXIX, Abstract #2421.
6. Amundsen, H. E. F. (1987). 'Evidence for liquid immiscibility in the upper mantle.' Nature, 327, 692-695.
7. McKay, D.S., E.K Gibson Jr., K.L. Thomas-Keptra, H. Vali, C.S. Romanek, S.J. Clemett, X. D.F. Chillier, C.R. Maechling and R.N. Zare (1996). 'Search for Past Life on Mars: Possible Relic Biogenic Activity in Martian Meteorite ALH84001.' Science 273, 924-930.
8. Treiman, A.H., H.E.F. Amundsen, David F. Blake and Ted Bunch (2002). 'Hydrothermal origin for carbonate globules in Martian meteorite ALH84001: a terrestrial analogue from Spitsbergen (Norway). EPSL 204 (2002), 323-332.
9. Harland, W.B. (1997). 'The Geology of Svalbard.' Memoir 17, Geological Society of London (521 p.).
10. Hausrath, E.M., Treiman, A., Bish, D.L., Blake, D., Sarrazin, P., Vincenzi, E., Midtkandl, I., Steele, A., and Brantley, S.L. (2009). 'Short and long-term olivine weathering in Svalbard, and implications for Mars.' Astrobiology 8(6), 1061-1069.
11. Treiman, A.H., K.L. Robinson, D.F. Blake and D. Bish (2010). 'Mineralogy Determinations by CheMin XRD, Tested on Ultramafic Rocks (Mantle Xenoliths).' AbSciCon 2010, Abstract #5351.
12. Blake, D.F., H.E.F. Amundsen, L. Benning, D. Bish, P. Conrad, M. Fogel, I. Midtkandal, D. Ming, A. Steele, A.H. Treiman and the AMASE team (2010). 'Carbonate cements from the Sverrefjell and Sigurdfjell volcanoes, Svalbard Norway; Terrestrial analogs for Martian carbonates?' AbSciCon 2010, Abstract #5119.
13. Schulte, M., D. Blake, T. Hoehler and T. McCollom (2006). 'Serpentinization and its implications for life on the early Earth and Mars.' J. Astrobiology 6(2), 364-376.
14. Steele, A., H.E.F. Amundsen, P.G. Conrad, L. Benning and the AMASE '09 Team (2010). 'Arctic Mars Analogue Svalbard Expedition (AMASE) 2009.' AbSciCon 2010, Abstract #5674.
15. Morris, R.V. et al (2010). 'Identification of Carbonate-Rich Outcrops on Mars by the Spirit Rover.' Sciencexpress, / www.sciencexpress.org / 3 June 2010 / Page 1-8 / 10.1126 / science / 1189667.
16. Sarrazin, P., P. Dera, R.T. Downs, D. Blake, D. Bish and M. Gailahou (2009). 'Hybrid X-ray Diffraction for Planetary Mineralogical Analysis of Unprepared Samples.' LPSC XXXX, Abstract #1496.
17. Wilkinson, M. (2010). 'Beyond Terra Firma.' Chemistry World, March 2010 pp. 50-53 (www.chemistryworld.org).
18. Marshall, A. (2009). 'The Fatal Consequences of Counterfeit Drugs.' Smithsonian Magazine, Oct. 2009; Finkle, M., (2007). 'Malaria: Stopping a Global Killer.' National Geographic, July, 2007.
19. Newton, P.N. et al (2008). 'A Collaborative Epidemiological Investigation into the Criminal Fake Artesunate Trade in South East Asia.' PLoS Medicine | www.plosmedicine.org, February 2008, Vol. 5, Issue 2, pp. 209-219.
20. Newton, P. N. et al (2006). 'Manslaughter by Fake Aretesunate in Asia - Will Africa Be Next? Plos Medeine 3(6):e197. DOI:10.1371 / Journal.pmed.0030197.
21. Blake, D.F., Philippe Sarrazin, Bradley W. Boyer and Tyler C. Jennison (2010). 'The use of field-portable p-XRD for the rapid identification of counterfeit pharmaceutical products and subsequent excipient identification and quantification.' PPXRD IX, Abstracts w/program, Hilton Head Island, SC.
22. http://www.inxitu.com/new/html/duetto.html, http://www.inxitu.com/images/Duettowhitepaper.pdf
23. Chiari, G. (2009) 'Saving Art in situ.' Nature Vol. 453, 159.
24. The author is grateful for nearly 20 years of support from NASA-sponsored research and SBIR activities that made this instrument possible. Thanks also to the many dedicated engineers, technicians, scientists and managers at the Jet Propulsion Laboratory, Pasadena, CA who made the CheMin FM a reality.

Appendices.

A. The CCD imager is operated in single photon counting mode (the CCD is exposed and read often enough so that in the vast majority of cases, pixels contain either background noise or the charge from a single photon). When a single X-ray photon is absorbed in a single pixel of the CCD, the energy of the photon is dissipated in the volume of the pixel as electron-hole pairs. Each electron-hole pair has about 3.65 eV of charge associated with it. The energies of X-ray photons from elements of geological interest

range from a few hundred to many thousands of electron volts. A calcium Kα x-ray fluoresced from the sample, for example, has an energy of 3.68 KeV, and would create slightly more than 1,000 electron hole pairs in the CCD. A cobalt Kα photon from the X-ray source that has an energy of 6.99 KeV, would produce 1,917 electron hole pairs in the sample.

B. A maximum of 65 mm3 of sample material is delivered to the piezoelectrically vibrated funnel system that penetrates through the rover deck (during the time period when CheMin is not receiving samples, the CheMin inlet is protected by a cover). The funnel contains a 1 mm mesh screen to keep larger than expected grains from entering the CheMin sample handling system. Grains that cannot pass through the screen will remain there for the duration of the mission (samples will have been prescreened first to150 µm that pass through the screen will pass into the upper reservoir portion of the sample cell, where they will remain until the cell is inverted and they are dumped into the sump. However, under nominal conditions, the funnel will only receive material that has passed through the CHIMRA's 150 µm sieve. For the lifetime of the mission, CheMin is required to accept and analyze material delivered from CHIMRA with no more than 5% internal contamination between samples. Self-generated contamination originates from material that has remained in the funnel from previously delivered samples (and co-mingled with subsequent samples), or from material that has remained in previously used analysis cells (each cell will be used two to three times to accommodate 74 analyses during the nominal mission). CheMin empties used sample cells by inverting and vibrating the cell into a sump inside the instrument. Contamination is reduced by sample dilution; aliquots of sample material can either be dumped into the funnel and delivered directly to the sump through a shunt in the wheel without entering a sample cell (to remove funnel contamination), or a previously used sample cell can be filled with an aliquot of sample material, shaken and emptied to the sump prior to receiving a second aliquot of sample for analysis (to remove sample cell contamination). This processes requires coordination with CHIMRA to deliver more than one aliquot of a given sample.

C. The collimated ~50 µm diameter X-ray beam illuminates the center of an 8 mm diameter, 175-µm thick sample cell bounded by 6 µm thick Mylar or Kapton windows. The sample introduced into the funnel consists of

During the moderate shaking which results in grain convection, it is possible that phase segregation will occur as a result of size or density differences between individual mineral grains. To reduce this problem CheMin can episodically use larger shaking amplitudes (we call this 'chaos mode') to homogenize particle size or density segregations in the sample chamber.

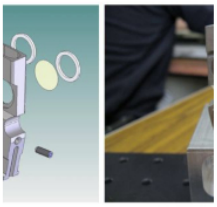

Figure 5

The CheMin sample cells are constructed in dual-cell 'tuning-fork' assemblies with a single horizontally driven piezoelectric actuator in each assembly (Fig. 5). Sixteen of the dual-cell assemblies are mounted around the circumference of the sample wheel. Five of the cells will be devoted to carrying standards; the other 27 cells are available for sample analysis and may be reused by dumping samples into the sump after analysis (Fig. 4).

Both Mylar and Kapton window cells are mounted on the wheel. Each window type has both benefits and drawbacks, and the choice of window type will be made based on the nature of the sample that is being analyzed. Mylar windows have a very flat diffraction background but Mylar is less durable than Kapton under severe vibration and is susceptible to destruction if highly acidic samples (e.g., the iron sulfate hydrate mineral copiapite) are analyzed. Kapton windows are extremely durable under severe vibration and are not susceptible to acid attack, but have a small diffraction contribution at ~6-7° 2θ (CoKα radiation) which could be mistaken for the (001) diffraction peak of some clay minerals. Windows of both Kapton (in 13 cells) and Mylar (in 14 cells) are used in the Flight Model (FM) and Development Model (DM), as shown in Fig. 4.

CheMin uses a 600x600 pixel E2V CCD-224 frame transfer imager operated with a 600x582 data collection area. The pixels in the array are 40x40 µm2, with an active region of deep depleted silicon 50 µms thick. The front surface passivation layer is thinned over a substantial fraction of the active pixel area. The E2V CCD-224 imager is a modern version of the E2V CCD-22 that was specially built for an X-ray astronomy application. The large size of the individual pixels causes a greater percentage of X-ray photons to dissipate their charge inside a single pixel rather than splitting the charge between pixels. The enhanced deep depletion zone results in improved charge collection efficiency for high energy X-rays. The thin passivation layer makes the CCD sensitive to relatively low-energy X-rays (AlKα at 1.49 KeV, SiKα at 1.75 KeV).

In order to keep the CCD from being exposed to photons in the visible energy range (from X-ray induced optical fluorescence from the sample) during analysis, a 150 nm Al film supported on a ~200 nm polyimide film is suspended in front of the detector. The detector itself is cooled to ~-60 °C by a cryocooler. The actual temperature of the CCD depends on the temperature of the RAMP (Rover Avionics Mounting Platform) into which the cryocooler's thermal load is dissipated. By cooling the CCD, dark current is reduced, as well as the effects of damage to the silicon lattice caused by neutrons from the RTG and the DAN instrument.

Figure and Table Captions

Figure 1. Geometry of the CheMin XRD/XRF instrument. a) (left) overall geometry of CheMin; b) (above right) XRD 2θ plot obtained by summing diffracted photons from the characteristic line of the X-ray source (colored magenta in Figure 1a); c) (below right) X-ray fluorescence spectrum obtained by summing all of the X-ray photons detected by the CCD (XRF photons from the sample shown schematically in green and red in Figure 1a).

Figure 2 (a). CheMin I instrument. A Princeton InstrumentsTM camera is interfaced to an evacuated sample chamber. A modified collimator from a Debye-Scherrer powder camera provided a 50 µm diameter collimated beam. X-rays are provided by a Norelco-Philips Tube tower. The detector is a Tektronix TK-512 backthinned, back illuminated 512 X 512 pixel CCD imager. Initially, analyses required several thousand CCD frames, with a total energy of thousands of watts hours. Since the sample chamber had to be taken apart to load samples, it typically took several days to align the X-ray beam after sample exchange. Power supplies, X-ray generator, camera controller and chilled water supplies for the X-ray tube tower and camera are not shown.

(b). CheMin II instrument. The instrument consisted of an AndorTM CCD camera interfaced to a sample chamber (kept at atmospheric pressure), bolted to an Oxford X-ray Technology Group micro-focus X-ray tube. The detector is an E2V 5530 1250 X 1150 pixel CCD imager. Samples could be exchanged in air, without disturbing the alignment of the instrument. Power supplies for the X-ray tube and camera are not shown. The instrument is air cooled.

(c). CheMin III. The instrument is shown in operation in Badwater Basin, Death Valley in 2003. The X-ray tube and camera are the same as used in CheMin II, however, miniature power supplies and camera control electronics are housed in a portable frame with the instrument. Samples are moved by piezo-shaking in a mylar film-bounded transmission cell. Not shown are storage batteries and laptop computer that provide power and instrument control. Data are collected as individual frames and analyzed off-line by the laptop computer.

(d). CheMin IV. (left) As deployed in Svalbard, Norway in 2006. (right) CheMin Co-I Dave Bish of Indiana University performs the first complete XRD/XRF data collection and quantitative analysis in the field. The instrument is fully self-contained, operated with an integrated computer and on-board lithium batteries and power supplies. Once an analysis is completed, the raw data are downloaded onto a USB storage drive and transferred to a laptop computer for processing.

Figure 3. Exploded view of CheMin spacecraft instrument. Major components of the instrument are labeled: (1), sample delivery funnel; (2), sample wheel containing 32 sample cells; (3), X-ray tube and collimator housed in pressurized SF6 dielectric (tube, collimator and 28 KV high voltage power supply weigh less than 1 Kg); (4), CCD imager with support structure; (5), CCD housing with cryocooler. Other components include electronics, sample wheel drive motor, etc. The entire instrument, which is essentially a 10' cube, weighs ~10 Kg and operates on ~40 watts.

Figure 4. Sample wheel. Sample cells (27 total) are loaded and analyzed at the top, then rotated 180 degrees and dumped in the sump after analysis. Permanent reference standards (5 total) are shown colored red, green cells are available for analysis of unknowns. The 'bypass cell,' shown in pink, is used to pass multiple sample aliquots through the funnel for contamination reduction by dilution. Similarly, individual sample cells can be loaded, shaken and dumped without analysis, then refilled to dilute any contamination that may be present in the cell from previous analyses. If necessary, cells can be used 3 or more times during the mission.

Figure 5. CheMin sample cells: (left), exploded view of dual-sample cell. Each dual-sample cell is a tuning fork driven at resonant frequency by a piezoelectric stack. The amplitude of shaking can be changed as a function of input voltage to the piezo. Each cell is an 8mm diameter X 170 µm thick volume bounded by X-ray transparent plastic films. During analysis, the piezo stack vibrates the cell at resonance, creating a turbulent flow of grains in the cell. Over time a myriad of grains from the sample flow past the 50 µm X-ray beam in random orientations. A reservoir above each sample cell holds excess material. The dual-cell assemblies are machined from solid titanium, and have a reproducible positioning accuracy (sample-to-detector path length) of less than 10 microns, 1/10th the diameter of a human hair).

Table 1. Diffraction pattern range and peak resolution (for CoKα radiation) of the CheMin FM. Range and resolution were chosen to allow for the successful identification and quantification of virtually all minerals.

Table 2. CheMin FM mineralogical analysis requirements. Analytical capabilities are defined by a 'flow down' of requirements derived from the science goals and objectives of the mission.

Figure 6 (a). Stack of raw single frames (10-second exposures) of 600X582 pixel CCD data. Each frame is background subtracted, and shows individual X-ray photon detections as white or gray spots. In any single exposure, only a few hundred pixels out of 350,000 record X-ray photon detections.

(b). Stack of energy-selected CoKα minor frames of CCD data. Each minor frame is a 600X582 array in which the x,y array elements store the integer sum of CoKα photons detected at that x,y pixel location during 100-200 individual frames (exposures).

(c). Major frame of CCD data, representing the sum of the minor frames. Major frames are used to construct a 2-D diffraction pattern that is translated into a more conventional 1-D diffractogram used for mineral identification and quantitative analysis. Minor frames are used to estimate the precision and accuracy of an analysis and to detect instrumental drift and transient anomalies in the data can be identified and removed.

(d). 1-D diffractogram constructed from a major frame of CCD data. Intensities from the 2-D pattern are summed circumferentially about the central beam to create an intensity vs. 2θ diffractogram, similar to that obtained in conventional powder X-ray diffractometry. The diffractogram shown is from the mineral amphibole, one of the reference standards in the CheMin FM.

(e). Raw Energy-Dispersive X-ray (EDX) histogram of a single frame of CCD data. The x-axis represents X-ray photon energy and the y-axis represents the number of counts per unit energy (in this case, represented as 'DN' or digital numbers from the CCD). Observed peaks include the primary CoKα flux at ~1960 DN, sample-generated FeKα at ~1890 DN, and sample-generated CaKα and CaKß at ~1525 and ~1640 DN respectively.

(f). Summed EDX histogram for major frame of CCD data. The X-axis is now converted from DN to energy in thousands of electron volts (KeV). Elemental peaks present include CoKα (6.92KeV), CoKß (7.70 KeV), FeKα (6.4 KeV), TiKα (4.51 KeV), TiKß (4.93 KeV), CaKα (3.68 KeV), CaKß (4.01 KeV), ArKα (2.96 KeV), SiKα (1.75 KeV) and AlKα (1.49 KeV). Fe, Ti and Ca are elements detected from the sample. Argon originates from the 10 mbar of Ar present in the FM during the analysis, Si originates from the detector itself and Al is generated from the light shield in front of the detector. The CheMin instrument is sensitive to elements above ~ Z=15 (phosphorus). While the CCD itself is supremely sensitive to low-energy X-rays such as AlKα, the transmission geometry of the instrument and the presence of a light shield precludes detection of these elements.
Figure 7. A synthetic ceramic was developed as a permanent standard for the instrument. This sample is used to measure the energy response of the CCD detector to sample-generated X-rays. X-ray sensitivity appears to be quite good from Sr to S (Al and Si are instrument generated). The FWHM of individual X-ray peaks, and ultimately X-ray detection and discrimination will be degraded by neutron damage from the RTG during the mission.

Figure 8. Use of Terra during NASA and other field campaigns. a). The author (NASA/ARC) during the Scarab/RESOLVE field test on Mauna Kea, HI (2008). Terra was used to analyze as-received volcanic soils and partial run products from In Situ Resource Utilization (ISRU) experiments. Lunar oxygen-generating equipment in the background b). Doug Ming (NASA/JSC) on an expedition to the dry valleys of Antarctica (2008). Terra was used to analyze soils and other materials to understand pedogenesis (soil generation) in cold, dry climates. c). Ron Peterson (Canadian Geological Survey), in the high Arctic of Canada (2009). Searching for low-temperature stability minerals such as the hydrates of iron and magnesium sulfate. d). The author (NASA/ARC) during the AMASE expedition in Svalbard, Norway (2009). Analyzing carbonate sediments and cements in volcanic vents for clues as to their origin.

Figure 9. Sverrefjell Volcano, Svalbard, Norway. Sverrefjell was apparently erupted under a thick ice sheet and later bisected by a km-thick glacier. Pillow lavas indicative of eruption at sea level or below are evident at several levels on the cindercone, and glacial eratics can be seen at all levels, including at the summit.

Figure 10. Volcanic vent. One wall of a breccia-filled vent showing carbonate cementation (orange) of the basaltic breccia. In all likelihood, original volcanic vents such as this one acted as a plumbing system for late stage hydrothermal systems under the ice. Large Norwegian (Hans Amundsen) shown for scale.

Figure 11. Cartoon of LUNA instrument. The LUNA instrument is a powder XRD with a reflection geometry. Angular range is 8-55° 2θ, sufficient to characterize all minerals thought to exist on the lunar surface.

Figure 12. Concept drawing of the hybrid single crystal Laue / powder XRD contact instrument. (left), Placement of detectors and X-ray source in the instrument. Fine-grained powders are characterized by powder XRD, similar to the LUNA instrument. Larger crystals are characterized by energy-resolved Laue single crystal patterns. (right), Placement of instrument on the arm of a mid-rover instrument similar to that proposed for the MAX-C 2018 mission to Mars.

Figure 13. Duetto Instrument with Mummy. Duetto, commissioned by the Getty Conservation Institute, is a commercial spinoff of CheMin, is used for in situ art characterization and art conservation.

Improving paleosol carbonate based estimates of ancient atmospheric CO2

Dan Breecker, Department of Geological Sciences, The University of Texas at Austin

Dan Breecker

Summary

The stable carbon isotope composition of calcium carbonate precipitated in soils (pedogenic carbonate) is controlled in part by the concentration of atmospheric CO_2 ($[CO_2]_{atm}$) during soil formation. Paleosol carbonates that escape alteration during burial diagenesis therefore preserve records of ancient $[CO_2]_{atm}$. However, in order to accurately reconstruct $[CO_2]_{atm}$ we must be able to accurately interpret the stable carbon isotope composition of pedogenic carbonate ($\delta^{13}C_{pc}$). Other variables such as temperature, moisture and soil CO_2 concentration that influence both calcite solubility and $\delta^{13}C_{pc}$ values vary greatly on a seasonal basis, especially in soils where pedogenic carbonate forms. We must therefore ask: what does the stable isotope composition of pedogenic carbonate record? The following discussion reviews recent advances in understanding the conditions under which calcium carbonate forms in modern soils, some of the implications of these findings and future research directions for further improvement of paleosol carbonate-based reconstructions of atmospheric CO_2.

Introduction

Paleosol carbonate records a wealth of information about ancient terrestrial environments. Modern pedogenic carbonate occurs, with few exceptions, only in climates with pronounced seasonal variations in precipitation minus evaporation. Therefore the sole presence of pedogenic carbonate in paleosols is an indicator of seasonal dryness and limited soil leaching. The depth of carbonate-bearing soil horizons is related to mean annual precipitation (Arkley, 1963; Gile, 1977; Jenny and Leonard, 1935; Retallack, 1994, 2005) although the significance of this relationship has been challenged (Royer, 1999) and it has been proposed that soil order-specific relationships are required (Nordt et al., 2006). The oxygen isotope composition of pedogenic carbonate is controlled by the oxygen isotope composition of precipitation (Cerling, 1984) and has been used to reconstruct the elevation history of large plateaus (e.g. Currie et al., 2005; Garzione et al., 2000; Ghosh et al., 2006b) and paleoatmospheric circulation (e.g. Amundson et al., 1996). The carbon isotope composition of pedogenic carbonate provides a record of vegetation in the past (Cerling, 1984, 1999) and has been used in numerous paleoecologic studies (e.g. Cerling and Hay, 1986; Fox and Koch, 2003; Kaakinen et al., 2006; Koch et al., 1995; Quade et al., 1989). Of particular interest in geochemistry, the carbon isotope composition of paleosol carbonate has also been used to reconstruct Phanerozoic atmospheric pCO_2 (e.g. Ekart et al., 1999 and references therein; Ghosh et al., 2001; Lee, 1999; Montañez et al., 2007; Nordt et al., 2002, 2003; Prochnow et al., 2006; Robinson et al., 2002). Quantifying $[CO_2]_{atm}$ through geologic time is widely important in studies of the geologic carbon cycle, the evolution of organisms, mass extinctions, and Earth's climate. This paper describes recent and future efforts to improve $[CO_2]_{atm}$ estimates using pedogenic carbonate.

The paleosol carbonate CO_2 barometer

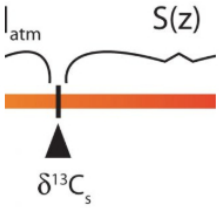

Figure 1

The paleosol carbonate CO_2 barometer or 'paleosol barometer' for short, although this name does not distinguish the technique from the similar but independent 'paleosol goethite CO_2 barometer' (Yapp and Poths, 1992), was developed by Thure Cerling in the 1990s. Cerling (1991; 1999) understood that CO_2 in soil pore spaces is a mixture between atmospheric and soil-derived (from autotrophic and heterotrophic soil respiration) components and recognized that if soil carbonate forms in carbon isotope equilibrium with soil CO_2 then the $\delta^{13}C$ value of soil carbonate is a function of the relative magnitude of the atmospheric and soil-respired components and their respective $\delta^{13}C$ values. The mass balance relationship is pictured graphically using the lever rule in Figure 1, from which it can be seen that:

$$\frac{\delta^{13}C_s - 1.0044\delta^{13}C_r - 4.4}{\delta^{13}C_a - \delta^{13}C_s} = \frac{[CO_2]_{atm}}{S(z)} \qquad 1)$$

where $S(z)$ is the soil-respired component of total CO_2 in the soil (i.e. $[CO_2]_{soil} = S(z) + [CO_2]_{atm}$) at depth z, $\delta^{13}C$ is the carbon isotope composition in standard delta notation, s, r and a refer to soil CO_2, soil-respired CO_2 and atmospheric CO_2, respectively, and the coefficient 1.0044 and the constant 4.4 derive from the difference in diffusivity between $^{13}CO_2$ and $^{12}CO_2$. The value of $\delta^{13}C_s$ in equation 1 is determined by using the temperature dependent carbon isotope fractionation factor (e.g. Romanek et al., 1992) to calculate the $\delta^{13}C$ value of CO_2 in equilibrium with the measured $\delta^{13}C$ value of paleosol carbonate ($\delta^{13}C_{pc}$). The $\delta^{13}C$ value of soil carbonate can therefore, in appropriate soils, be used to calculate $[CO_2]_{atm}$ using the following equation which is simply rearranged from equation 1 (Cerling, 1999):

$$[CO_2]_{atm} = S(z)\frac{\delta^{13}C_s - 1.0044\delta^{13}C_r - 4.4}{\delta^{13}C_a - \delta^{13}C_s} \qquad 2)$$

Equation 2 has been used to reconstruct $[CO_2]_{atm}$ for many time periods during the past 400 million years of Earth's history (e.g. Ekart et al., 1999).

The formation of pedogenic carbonate

In order to assign values to the variables on the right hand side of equation 2, it is typically assumed

About the Author

Dan Breecker is an assistant professor in the Department of Geological Sciences at the University of Texas at Austin.

He received a Ph.D. from the University of New Mexico in 2008 and was an NSF Earth Science Post Doctoral Fellow at the University of Arizona for one year before arriving at UT. His primary research interest involve the relationships between soils and climate and the gas chemistry of soils and caves.

In order to assign values to the variables on the right hand side of equation 2, it is typically assumed that paleosol carbonate formed at temperatures and soil CO_2 concentrations characterized by *mean* growing season conditions observed in modern soils (Cerling, 1991). However, recent work indicates that pedogenic carbonate does not form during mean growing season conditions, but instead forms during droughts (Breecker et al., 2009). In that study, the $\delta^{13}C$ values of soil CO_2 in modern soils from New Mexico, USA were generally lower than values in equilibrium with soil carbonate and only approached equilibrium values after an extended two month drought (typical of spring in New Mexico). The timing of carbon isotope equilibrium between soil CO_2 and soil carbonate was interpreted to identify the timing of carbonate formation. This interpretation requires the assumption that soil carbonate forms in carbon isotope equilibrium with soil CO_2, which is theoretically justified (Cerling and Quade, 1993), but remains to be experimentally or empirically demonstrated. However, the interpretation based on isotope equilibrium that pedogenic carbonate forms during warm, dry episodes is strongly supported by thermodynamic considerations: precipitation of carbonate in soils is driven by increasing temperature, increasing Ca^{2+} activity as a result of evapotranspiration, and decreasing soil pCO_2, caused by deceasing soil respiration rates as a result of water stress on plants and soil microorganisms.

A recently developed geothermometer that is based on the concentration of ^{13}C-^{18}O bonds in calcite (the 'clumped isotope thermometer') (Ghosh et al., 2006a; Schauble et al., 2006) is useful for investigating pedogenic carbonate formation. The formation temperatures determined using the clumped isotope thermometer of modern pedogenic carbonates collected at depths in excess of 50 cm are approximately equal to the mean air temperature during the warmest consecutive three months of the year (Passey et al., 2010). These high temperatures at depth during carbonate formation likely result from radiative heating of the soil surface as the soil dries and latent heat flux decreases and support the conclusion of Breecker et al (2009).

The conclusion that soil carbonate forms under conditions of water stress suggests that the *S(z)* values typically used in the paleosol barometer are higher than those appropriate for carbonate formation, which has resulted in substantial overestimation of paleoatmospheric CO_2 (Breecker et al., 2010). Revised paleoatmospheric CO_2 concentrations, determined using a more realistic *S(z)* value that is based on the study of modern soils, suggest that Earth's maximum persistent atmospheric CO_2 levels during the past 400 million years were in the range of 1000 ± 200 ppmV and that CO_2 levels similar to those predicted for the end of this century (800-1000 ppmV, estimated by the IPCC using SRES emission scenario A2 (Meehl et al., 2007)) may have forced Mesozoic greenhouse climate warmth (Breecker et al., 2010). The importance of this conclusion demands it be rigorously tested.

Breecker et al. (2010) used a single *S(z)* value for all paleosols which probably results in accurate estimates of mean $[CO_2]_{atm}$ calculated from large numbers of paleosols, but is probably not appropriate for every individual paleosol. Determining *S(z)* values that are appropriate for individual paleosols is a crucial step in improving the accuracy and temporal resolution of $[CO_2]_{atm}$ records. Progress on this front was made by a recent study in which *S(z)* values varied with paleosol morphology (Montañez et al., 2007). It has been reported that *S(z)* values correlate with, and may partly control, the depth from the soil surface to the carbonate-bearing horizon (Bk horizon), for a small but geographically diverse sample of modern soils (Retallack, 2009). This type of relationship may eventually be useful for assigning *S(z)* values to individual paleosols if it is calibrated for the seasonal timing of carbonate formation and if other variables that influence the depth to the Bk horizon (e.g. soil texture, parent material) can be accounted for.

Uncertainty of paleoatmospheric CO_2 estimates

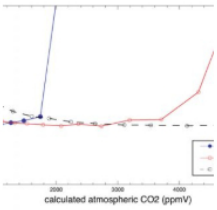

Figure 2

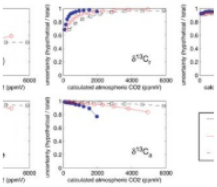

Figure 3

Here I use Monte Carlo simulations to investigate the how uncertainty in each of the variables on the right hand side of equation 2 (including temperature, which is used to calculate $\delta^{13}C_s$) influences uncertainty in the calculated values of $[CO_2]_{atm}$. Figure 2 is a plot of the estimated total uncertainty of $[CO_2]_{atm}$ calculated using equation 2. Figure 3 illustrates the degree to which the total uncertainty is reduced if the value of one of the variables in equation 2 is known exactly.

Simulated uncertainties vary with the calculated values of $[CO_2]_{atm}$ (Figures 2 & 3). The total uncertainties decrease as values of $[CO_2]_{atm}$ approach values of *S(z)* (Figure 2). When $S(z) \approx [CO_2]_{atm}$ (the zones of minimum total uncertainty in Figure 1) calculated uncertainties are also more sensitive to *S(z)* than they are to any of the other variables in equation 2 (i.e. exact values of *S(z)* reduce uncertainty more than exact values of any of the other variables do) (Figure 3). Sensitivity to $\delta^{13}C_r$ increases as the ratio of mean values $[CO_2]_{atm}/S(z)$ decreases and sensitivity to $\delta^{13}C_a$ increases as $[CO_2]_{atm}/S(z)$ increases (Figure 3). These results are expected based on the lever rule: the relative magnitude of $[CO_2]_{atm}$ and *S(z)* is impacted more by changes on the short end than on the long end of the lever. The decreases in uncertainty resulting from knowing exact values of temperature and $\delta^{13}C_{pc}$ are small (Figure 3) because the value of $\delta^{13}C_s$ is relatively insensitive to temperature and the value of $\delta^{13}C_{pc}$ is generally well constrained (i.e. $\delta^{13}C_{pc}$ was assigned a small error in this analysis). Therefore, the clumped isotope thermometer is not expected to improve the uncertainty of $[CO_2]_{atm}$ calculated using the paleosol barometer, although it is promising for the quantification of soil and maximum air paleotemperatures (Passey et al., 2010).

The results of the Monte Carlo simulations indicate that selecting paleosols for which appropriate *S(z)* values are similar to contemporaneous $[CO_2]_{atm}$ values will improve uncertainty. Inspecting Figure 2 indicates that the total uncertainty is less than 80% of the average calculated value of $[CO_2]_{atm}$ when $[CO_2]_{atm}/S(z)$ is between the values of 0.3 and 1.8. Total uncertainty increases sharply for $[CO_2]_{atm}/S(z)$ outside this range (Figure 2). Therefore, using equation 1, paleosols that will result in the lowest uncertainty can be identified, without needing to assume values for $[CO_2]_{atm}$ or *S(z)*, by assuring that the following holds true for the applicable $\delta^{13}C$ values:

$$0.3 < \frac{\delta^{13}C_s - 1.0044\delta^{13}C_r - 4.4}{\delta^{13}C_a - \delta^{13}C_s} < 1.8 \qquad 3)$$

The results of the Monte Carlo simulations also indicate that better estimates of $\delta^{13}C_r$ may be required to improve estimates for time periods when $[CO_2]_{atm}$ was below ~500 ppmV. This is especially true if water stress is found to have a substantial impact on $\delta^{13}C_r$ values in calcic soils as hypothesized below. These conclusions are intended to motivate and direct future research.

Calibrating the barometer

The paleosol carbonate CO_2 barometer can be calibrated by studying modern calcic soils. Application of

The paleosol carbonate CO_2 barometer can be calibrated by studying modern calcic soils. Application of the barometer to Holocene soils (for which the correct atmospheric CO_2 concentrations are preindustrial values) is a reasonable but somewhat blind calibration technique in that it does not address process nor does it allow independent calibration of each variable in equation 2. Monitoring seasonal variation in variables such as soil temperature, soil moisture, soil CO_2 concentration and the stable isotope composition of soil CO_2 will help establish the timing and mechanism of carbonate formation and help assign values for T, $\delta^{13}C_r$ and *S(z)* that are appropriate in equation 2. The discussion of model sensitivity above indicates that efforts are most worthwhile spent on improving estimates of *S(z)* and $\delta^{13}C_r$. Interestingly, it appears that there may be room for improvement in both of these variables.

Soil CO_2 concentrations vary greatly among different soils and seasonally within the same soil. *S(z)* values that correspond to carbonate formation have not been widely identified. Ongoing work on a variety of modern soils will help refine *S(z)* values appropriate for different paleosol types. Vertisols (soils in which shrinking and swelling of clays dominate morphological development) and soils with vertic properties are commonly preserved in the geologic record. Vertisols Therefore, my group at UT and a group at Baylor University led by Drs. Steve Driese and Lee Nordt are together currently studying soil CO_2 and pedogenic carbonate in modern Vertisols from central and south Texas. These Vertisols are particularly good modern analogs for many paleo-Vertisols used to reconstruct ancient $[CO_2]_{atm}$ (e.g. Mora and Driese, 1999; Mora et al., 1996; Nordt et al., 2002, 2003). Our hypothesis is that cracking of these smectite-rich soils upon drying opens conduits for the release of CO_2 from the soil, resulting in a large decrease in soil CO_2 concentration, which in turn drives calcite precipitation. We suspect that decreasing soil respiration rates, increased pore space volume, increased diffusivity and barometric pumping through cracked soil all influence the dynamics of soil CO_2 in Vertisols. Understanding the processes involved in carbonate formation and soil CO_2 variations may help establish proxies for *S(z)* and $\delta^{13}C_r$.

Values for $\delta^{13}C_r$ in equation 2 are typically assumed to equal the $\delta^{13}C$ value of well-preserved, contemporaneous terrestrial organic material (e.g. Montañez et al., 2007; Nordt et al., 2002), or are calculated from the $\delta^{13}C$ value of contemporaneous marine carbonate assuming a constant carbon isotope fractionation between the ocean and the atmosphere and between the atmosphere and vegetation (e.g. Ekart et al., 1999; Nordt et al., 2003). However, it is well known that there is a wide range in the $\delta^{13}C$ value of C_3 plants (Deines, 1980), resulting at least in part from the effect of water stress on the magnitude of photosynthetic discrimination (Farquhar et al., 1989). Water stress, which tends to occur in the seasonally dry climates in which pedogenic carbonates form, can substantially increase the $\delta^{13}C$ values of plants and can even result in substantial (~2‰) differences in the $\delta^{13}C$ value of the leaves of individual species growing along local soil moisture gradients (e.g. Ehleringer and Cooper, 1988). Terrestrial organic materials are typically well-preserved where they were protected from degradation in rapidly aggrading sediments or anoxic, water-saturated environments such as swamps. Unfortunately this creates a preservation bias toward plant material that is less water stressed when compared with the vegetation that was probably growing in calcic soils. Furthermore, approximately half of the CO_2 respired in soils is generated in the rhizosphere (root zone) (Hanson et al., 2000) where the substrate consists largely of recently assimilated carbon (Ekblad and Högberg, 2001; Högberg et al., 2001). Therefore, $\delta^{13}C$ values of rhizosphere-respired CO_2 vary seasonally and are highest when vegetation is water stressed and pedogenic carbonate is forming. These considerations suggest that the $\delta^{13}C$ value of respired CO_2 in calcic paleosols was higher than the $\delta^{13}C$ value of well-preserved organic matter in sedimentary successions. However, there is considerable direct evidence for a kinetic isotope fractionation during microbial decomposition of organic matter, which results in production of ^{13}C-depleted CO_2 (e.g. Blair et al., 1985; Mary et al., 1992) and therefore may somewhat compensate for the moisture-related effects described above. Finding a proxy for $\delta^{13}C_r$ values that correspond to the seasonal timing of carbonate formation is a challenge for future research. A proxy for $\delta^{13}C_r$ would help improve estimates of low atmospheric CO_2 concentrations during Earth's past, which are particularly important for determining the threshold CO_2 concentrations for continental glaciation (Royer, 2006).

Concluding Remarks

Soils are complicated natural systems. Simplifying our view of soils so that it is necessary and sufficient for the accurate interpretation of paleosols constitutes an ongoing challenge. Previous research has made great strides toward this end as evidenced by the emerging consensus among different techniques for reconstructing ancient $[CO_2]_{atm}$. The discussion above is intended to build on previous work by highlighting certain complexities that may be worth considering in future applications of the paleosol carbonate CO_2 barometer. Process-based proxy calibration studies can provide uniformitarian insight and are one way forward that should be encouraged.

Acknowledgements

I thank T. Cerling for inspiration, Z. Sharp, L. McFadden and J. Quade for their outstanding mentorship and G. Davidson for a helpful review.

References

Amundson, R., Chadwick, O., Kendall, C., Wang, Y., and DeNiro, M., 1996, Isotopic evidence for shifts in atmospheric circulation patterns during the late Quaternary in mid-North America: Geology, v. 24, p. 23-26.

Arkley, R.J., 1963, Calculation of carbonate and water movement in soil from climatic data: Soil Science, v. 96, p. 239-248.

Blair, N., Leu, A., Muñoz, E., Olsen, J., Kwong, E., and des Marais, D., 1985, Carbon isotopic fractionation in heterotrophic microbial metabolism: Applied and Environmental Microbiology, v. 50, p. 996-1001.

Breecker, D., Sharp, Z.D., and McFadden, L., 2009, Seasonal bias in the formation and stable isotope composition of pedogenic carbonate in modern soils from central New Mexico, USA: Geological Society of America Bulletin, v. 121, p. 630-640.

Breecker, D.O., Sharp, Z.D., and McFadden, L.D., 2010, Atmospheric CO_2 concentrations during ancient greenhouse climates were similar to those predicted for A.D. 2100.: Proceedings of the National Academy of Sciences of the United States of America, v. 107, p. 576-580.

Cerling, T.E., 1984, The stable isotopic composition of modern soil carbonate and its relationship to climate: Earth and Planetary Science Letters, v. 71, p. 229-240.

-, 1991, Carbon dioxide in the atmosphere: Evidence from Cenozoic and Mesozoic paleosols: American Journal of Science, v. 291, p. 377-400.

-, 1999, Stable carbon isotopes in palaeosol carbonates, *in* M. Thiry, R.S.-C., ed., Palaeoweathering, palaeosurfaces and related continental deposits. Special Publication of the International Association of Sedimentologists, Volume 27, p. 43-60.

Cerling, T.E., and Hay, R.L., 1986, An isotopic study of paleosol carbonates from Olduvai Gorge: Quaternary Research, v. 25, p. 63-78.

Cerling, T.E., and Quade, J., 1993, Stable carbon and oxygen isotopes in soil carbonates, *in* Swart, P.K., Lohmann, K.C., McKenzie, J., and Savin, S., eds., Climate Change in Continental Isotopic Records: Geophysical Monograph 78, American Geophysical Union, p. 217-231.

Currie, B.S., Rowley, D.B., and Tabor, N.J., 2005, Middle Miocene paleoaltimetry of southern Tibet: Implications for the role of mantle thickening and delamination in the Himalayan orogen: Geology, v. 33, p. 181-184.

Deines, P., 1980, The isotopic composition of reduced organic carbon, *in* Fritz, P., and Fontes, J.C., eds., Handbook of Environmental Isotope Geochemistry, Volume 1: Amsterdam, Elsevier, p. 329-406.

Ehleringer, J.R., and Cooper, T.A., 1988, Correlations between carbon isotope ratio and microhabitat in desert plants: Oecologia, v. 76, p. 562-566.

Ekart, D.D., Cerling, T.E., Montañez, I.P., and Tabor, N.J., 1999, A 400 million year carbon isotope record of pedogenic carbonate: Implications for paleoatmospheric carbon dioxide: American Journal of Science, v. 299, p. 805-827.

Ekblad, A., and Högberg, P., 2001, Natural abundance of ^{13}C in CO_2 respired from forest soils reveals speed of link between tree photosynthesis and root respiration: Oecologia, v. 127, p. 305-308.

Farquhar, G.D., Ehleringer, J.R., and Hubick, K.T., 1989, Carbon isotope discrimination and photosynthesis: Annual Review of Plant Physiology and Plant Molecular Biology, v. 40, p. 503-537.

Fox, D., and Koch, P.L., 2003, Tertiary history of C_4 biomass in the Great Plains, USA: Geology, v. 31, p. 809-812.

Garzione, C.N., Quade, J., DeCelles, P.G., and English, N.B., 2000, Predicting paleoelevation of Tibet and the Himalaya from $\delta^{18}O$ vs. altitude gradients in meteoric water across the Nepal Himalaya: Earth and Planetary Science Letters, v. 183, p. 215-229.

Ghosh, P., Adkins, J., Affek, H., Balta, B., Guo, W., Schauble, E.A., Schrag, D., and Eiler, J.M., 2006a, ^{13}C-^{18}O bonds in carbonate minerals: a new kind of paleothermometer: Geochimica et Cosmochimica Acta, v. 70, p. 1439-1456.

Ghosh, P., Garzione, C.N., and Eiler, J.M., 2006b, Rapid uplift of the Altiplano revealed through ^{13}C-^{18}O bonds in paleosol carbonates: Science, v. 311, p. 511-515.

Ghosh, P., Ghosh, P., and Bhattacharya, S.K., 2001, CO_2 levels in the late Palaeozoic and Mesozoic atmosphere from soil carbonate and organic matter, Satpura basin, Central India: Palaeogeography, Palaeoclimatology, Palaeoecology, v. 170, p. 219-236.

Gile, L.H., 1977, Holocene soils and soil-geomorphic relations in a semiarid region of southern New Mexico: Quaternary Research, v. 7, p. 112-132.

Hanson, P.J., Edwards, N.T., Garten, C.T., and Andrews, J.A., 2000, Separating root and soil microbial contribution to soil respiration: A review of methods and observations: Biogeochemistry, v. 48, p. 115-146.

Högberg, P., Nordgren, A., Buchmann, N., Taylor, A.F.S., Ekblad, A., Högberg, M.N., Nyberg, G., Ottosson-Löfvenius, M., and Read, D.J., 2001, Large scale forest girdling shows that current photosynthesis drives soil respiration: Nature, v. 411, p. 789-792.

Jenny, H.J., and Leonard, C.D., 1935, Functional relationships between soil properties and rainfall: Soil Science, v. 38, p. 363-381.

Kaakinen, A., Sonninen, E., and Lunkka, J.P., 2006, Stable isotope record in paleosol carbonates from the Chinese Loess Plateau: Implications for late Neogene paleoclimate and paleovegetation: Palaeogeography, Palaeoclimatology, Palaeoecology, v. 237, p. 359-369.

Koch, P.L., Zachos, J.C., and Dettman, D.L., 1995, Stable isotope stratigraphy and paleoclimatology of the Paleogene Bighorn Basin (Wyoming, USA): Palaeogeography, Palaeoclimatology, Palaeoecology, v. 115, p. 61-89.

Lee, Y.I., 1999, Stable isotopic composition of calcic paleosols of the early Cretaceous Hasandong Formation, southeatern Korea: Palaeogeography, Palaeoclimatology, Palaeoecology, v. 150, p. 123-133.

Mary, B., Mariotti, A., and Morel, J.L., 1992, Use of ^{13}C variations at naural abundance for studying the biodegradation of root mucilage, roots an glucose in soil: Soil Biology and Biochemistry, v. 24, p. 1065-1072.

Meehl, G.A., Stocker, T.F., Collins, W.D., Friedlingstein, P., Gaye, A.T., Gregory, J.M., Kitoh, A., Knutti, R., Murphy, J.M., Noda, A., Raper, S.C.B., Watterson, I.G., Weaver, A.J., and Zhao, Z.-C., 2007, Global Climate Projections, *in* Solomon, S., Qin, D., Manning, M., Chen, Z., Marquis, M., Averyt, K.B., Tignor, M., and Miller, H.L., eds., Climate Change 2007: The Physcial Science Basis. Contribution of Working Group I to the Fourth Assessment Report of the Intergovernmental Panel on Climate Change: Cambridge, Cambridge Univ. Press, p. 747-845.

Montañez, I.P., Tabor, N.J., Niemeler, D., DiMichele, W.A., Frank, T.D., Fielding, C.R., Isbell, J.L., Birgenheier, L.P., and Rygel, M.C., 2007, CO_2-forced climate and vegetation instability during late Paleozoic deglaciation: Science, v. 315, p. 87-91.

Mora, C.I., and Driese, S.G., 1999, Palaeoclimatic significance and stable carbon isotopes of Paleozoic red bed paleosols, Appalachain Basin, USA and Canada, *in* Thiry, M., and Simon-Coinçon, R., eds., Palaeoweathering, Palaeosurfaces and Related Continental Deposits: International Association of Sedimentologists Special Publication No. 27, p. 61-84.

Mora, C.I., Driese, S.G., and Colarusso, L.A., 1996, Middle to Late Paleozoic atmospheric CO_2 levels from soil carbonate and organic matter: Science, v. 271, p. 1105-1107.

Nordt, L., Atchley, S., and Dworkin, S.I., 2002, Paleosol barometer indicates extreme fluctuations in atmospheric CO_2 across the Creatceous-Tertiary boundary: Geology, v. 30, p. 703-706.

-, 2003, Terrestrial evidence for two greenhouse events in the latest Cretaceous: GSA Today, v. 13, p. 4-9.

Nordt, L., Orosz, M., Driese, S.G., and Tubbs, J., 2006, Vertisol carbonate properties in relation to mean annual precipitation: Implications for paleoprecipitation estimates: Journal of Geology, v. 114, p. 501-510.

Passey, B.H., Levin, N.E., Cerling, T.E., Brown, F.H., and Eiler, J.M., 2010, High temperature environments of human evolution in East Africa based on bond ordering in paleosol carbonates: Proceedings of the National Academy of Science of the United States of America, v. 107, p. 11245-11249.

Prochnow, S.J., Nordt, L., Atchley, S., and Hudec, M.R., 2006, Multi-proxy evidence for middle and late Trassic climate trends in eastern Utah: Palaeogeography, Palaeoclimatology, Palaeoecology, v. 232, p. 53-72.

Quade, J., Cerling, T.E., and Bowman, J.R., 1989, Development of the Asian monsoon revealed by marked ecological shift during the latest Miocene in northern Pakistan: Nature, v. 342, p. 163-166.

Retallack, G.J., 1994, The environmental factor approach to the interpretation of paleosols, *in* Amundson, R., ed., Factors of soil formation: A fiftieth anniversary retrospective: Soil Science Society of America Special Publication 33, p. 31-64.

-, 2005, Pedogenic carbonate proxies for amount and seasonality of precipitation in paleosols: Geology, v. 33, p. 333-336.

-, 2009, Refining a pedogenic-carbonate CO_2 paleobarometer to quantify a middle Miocene greenhouse spike: Palaeogeography, Palaeoclimatology, Palaeoecology, v. 281, p. 57-65.

Robinson, S.A., Andrews, J.E., Hesselbo, S.P., Radley, J.D., Dennis, P.F., Harding, I.C., and Allen, P., 2002, Atmospheric pCO_2 and depositional environment from stable-isotope geochemistry of calcrete nodules (Barremian, lower Cretaceous, Wealden Beds, England): Journal of the Geological Society, London, v. 159, p. 215-224.

Romanek, C.S., Grossman, E.L., and Morse, J.W., 1992, Carbon isotopic fractionation in synthetic aragonite and calcite - effect of temperature and precipitation rate: Geochimica et Cosmochimica Acta, v. 56, p. 419-430.

Royer, D.L., 1999, Depth to pedogenic carbonate horizon as a paleoprecipitation indicator?: Geology, v. 27, p. 1123-1126.
-, 2006, CO_2-forced climate thresholds during the Phanerozoic: Geochimica et Cosmochimica Acta, v. 70, p. 5665-5675.

Schauble, E.A., Ghosh, P., and Eiler, J.M., 2006, Preferential formation of ^{13}C-^{18}O bonds in carbonate minerals, estimated using first-principles lattice dynamics: Geochimica et Cosmochimica Acta, v. 70, p. 2510-2529.

Yapp, C.J., and Poths, H., 1992, Ancient atmospheric CO_2 pressures inferred from natural goethites: Nature, v. 355, p. 342-344.

Figure 1. A graphical representation of the lever rule as applied to the paleosol barometer. $\delta^{13}C_r{}^*$ represents the diffusion-modified $\delta^{13}C$ value of the soil-derived endmember and equals $1.0044\delta^{13}C_r + 4.4$. The magnitude of $[CO_2]_{atm}$ and $S(z)$ are proportional to the distances along the lever, or differences in δ values, as labeled. Equation 1 can be written directly from the relationship shown.

Figure 2. Monte Carlo simulations of the uncertainty of calculated atmospheric CO_2 concentrations. 10,000 values were randomly selected from each of the following normal distributions (mean ± standard deviation) and used to calculate atmospheric CO_2 concentrations with equation 2: $\delta^{13}C_r$ = -26 ± 1‰, $\delta^{13}C_a$ = -6.5 ± 1‰, temperature = 25 ± 5°C, $S(z)$ = 1000, 2500 or 5000 ± 50%. A range of mean $\delta^{13}C_{pc}$ values between -3 and -12‰ (± 0.5‰) were used to calculate a range of mean atmospheric CO_2 concentrations (x-axis) for each mean $S(z)$ value. The total uncertainty was estimated by calculating the standard deviation (1σ) of each set of 10,000 atmospheric CO_2 concentrations and is expressed as a percentage of the mean calculated value of $[CO_2]_{atm}$.

Figure 3. Monte Carlo simulations of the effect of each variable in equation 2 on the total uncertainty. The y-axis is the ratio of the uncertainty calculated when the value of one of the variables (labeled on each plot) is known exactly to the total uncertainty from Figure 2.

Titan: The Enduring Enigma

Conor Nixon, NASA Goddard Space Flight Center

Conor Nixon

About the Author

Conor Nixon is a planetary scientist based at NASA Goddard Space Flight Center in Maryland. His primary research involves the use of the mid-infrared spectrometer (CIRS) on the Cassini spacecraft to study the planetary atmospheres of Jupiter, Saturn and its moon Titan, with particular emphasis on chemical composition. He has also measured stable isotopic ratios in these atmospheres to study their origin and evolution. Prior to arriving at NASA, Dr. Nixon obtained a D. Phil. from the University of Oxford, England in Atmospheric Physics.

1. Introduction

Titan has both fascinated and perplexed scientists since its discovery in 1655 by the Dutch astronomer Christiaan Huygens, especially due to its distinct orange coloration and lack of visible surface features. Little progress was made on understanding this satellite until 1944, with the breakthrough discovery of methane gas absorptions by G. P. Kuiper (1944), confirming earlier suspicions of an atmosphere by Josep Comas Sola (1908). Titan was now unique - the only moon in the solar system with a substantial atmosphere - and yet this only added to the mystery, as the depth of the atmosphere and hence the diameter of the body was now unknown. At last in 1979 the Voyager 1 spacecraft flew behind Titan as seen from Earth, and scientists were able to use the occultation of the radio signal to determine where the solid surface began. The answer: a diameter of 5150 km, slightly smaller than Jupiter's moon Ganymede but larger than the planet Mercury (Lindal et al. 1983). In addition, Voyager showed that methane constitutes just 5% of the bulk atmosphere, with molecular nitrogen (N2) making up the remaining 95%.

Figure 1

Voyager however was unable to image the surface: its cameras could not penetrate the haze blanket any more than Earth-based telescopes, and no hoped-for gaps in the veil were seen. To delve deeper, a new mission was planned: the double act of Cassini [Fig. 1], a Saturn-orbiting mother ship, and Huygens, a dedicated Titan atmospheric probe that was also hoped to survive a parachute landing on the surface. Here another of Titan's unending mysteries became an engineering dilemma: what sort of surface would Huygens land on? In the post-Voyager years, models of Titan's chemistry showed that vast quantities of hydrocarbons, especially ethane gas, are being continuously generated in the upper atmosphere (Yung et al. 1984). These percolate down to the lower atmosphere encountering a temperature minimum at 45 km, the tropopause, where they condense and rain out onto the surface [Fig. 2]. Over billions of year of production, the surface could now be covered in oceans of exotic liquids (Flasar 1983; Lunine et al. 1983).

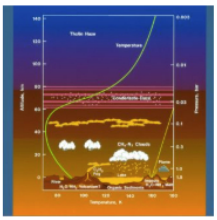

Figure 2

The year is now 2010, and Huygens successfully landed on Titan in January 2005, returning dramatic new insights during its brief mission of a few hours. Cassini has been orbiting Saturn for 6 years, making 70 close flybys of Titan to date, and returned a wealth of information regarding the enigmatic moon, answering some questions but raising many more in their place. The mission has now been extended for a further 7 years and as we stand now at the mid-point of this incredible journey, it is appropriate to both reflect on how far along the road to understanding Titan we have come, and what tasks lie on the road ahead.

In this article I have selected two key scientific mysteries about Titan that Cassini-Huygens was designed to shed light on, and show how the first of these has been mostly solved - although it has raised new questions. Meanwhile the second puzzle initially showed promising signs of a solution as well, but as the mission progressed these first diagnoses were shown to be off the mark, and now the problem stands deeper and more perplexing than ever. In the closing, I will mention other unsolved riddles that may be answered during the remainder of the mission, or may await focused future missions. One thing about Titan is certain: that there will be no shortage of mysteries for a long time to come.

2.1 Wet or dry?

Since the 1970s it had been suggested that methane, and perhaps other organic chemicals detected in Titan's atmosphere would collect on the surface, forming solid or liquid deposits. In the post-Voyager era these ideas firmly took root, and initial studies predicted that the satellite could be covered by a layer of liquid methane or ethane to a mean depth of up to 600m (Flasar 1983; Lunine et al. 1983). However, contrary evidence soon emerged. One problem was Titan's non-zero eccentricity, as the orbit would tend to circularize over geologic time if the tides raised in large, shallow oceans were able to dissipate against landmasses. This reasoning implied that the liquid covering must either be deep and global, or limited to small isolated lakes (Sagan and Dermott 1982). To distinguish between these scenarios, a dedicated effort was made to measure Titan's radar reflectivity, which showed relatively high values incompatible with a deep global ocean (Muhleman et al. 1990).

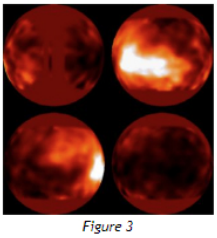

Figure 3

During the 1990s, a breakthrough technique finally allowed the surface to be imaged at short wavelengths. By exploiting spectral 'windows' in the near-infrared, where methane gas was transparent, large telescopes equipped with adaptive optics were able to observe a bright 'continent' on the leading hemisphere, and also to confirm that Titan was indeed synchronously rotating, keeping the same face towards Saturn at all times (Smith et al. 1996; Combes et al. 1997; Meier et al. 2000; Coustenis et al. 2001) [Fig. 3]. Most moons in the solar system are 'tidally locked' in this way, including the Earth's own Moon. But once again there was no evidence for widespread seas or oceans. The final surprise before Cassini was a second radar experiment, using the giant 305m dish at Arecibo to transmit and receive, that found the tell-tale specular reflection often characteristic of liquid surfaces (similar to the glint of the Sun on the sea) in about 75% of locations (Campbell et al. 2003): a confusing result given the accumulated evidence militating against large bodies of liquid at this point.

This then was the prevailing paradigm prior to the arrival of Cassini-Huygens in 2004: Titan appeared to have a heterogeneous, surprisingly reflective surface, albeit devoid of widespread oceans. Yet tantalizing clues hinted at the existence of localized surface liquids. Now it would be up to Cassini and Huygens to resolve the question conclusively.

The first round went to Huygens, which landed on Titan on January 14th 2005. Images snapped during the descent showed an intriguing landscape, with brighter 'highlands' apparently threaded by dendritic

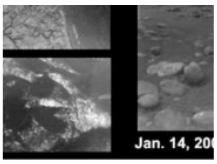

Figure 4

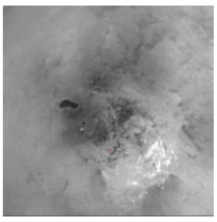
Figure 5

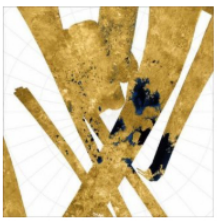
Figure 6

(branching) networks of channels, and darker lowlands, where Huygens eventually settled, scattered with stream-tossed cobbles of ice like the outwash from a flood [Fig. 4]. Yet no evidence for running rivers or standing lakes, not even a pond, was seen by Huygens. Was Titan then akin to Mars, where a rain-drenched past had given way long ago to dried-up deserts? The answer was not long in coming.

In June that same year, the long-awaited 'aha' moment arrived. During an un-targeted distant flyby, Cassini obtained the first good view of Titan's south pole, and its imaging cameras spied a striking dark outline in the shape of a titanic footprint 235 km across and 20,000 km2 in area located at 72°S [Fig. 5]. Later observations confirmed the diagnosis, and the feature was later named Ontario Lacus. So perhaps lakes were a polar phenomenon only, where the global circulation might bring hydrocarbon-saturated air to colder climes where condensation and rainfall could occur? Would lakes also be discovered on the opposite pole? Unfortunately, Titan's far north would be shadowed in the long polar night for years to come, so visible-light cameras were temporarily blind.

So it fell to Cassini's synthetic aperture radar (SAR) to discover the biggest wetlands of all: the vast expanses of seas and lakes first recorded during a polar pass in July 2006. These radar-dark features showed almost no backscatter of radio waves to spacecraft, and were compatible only with an interpretation of a smooth liquid surface (Stofan et al. 2007). Later passes revealed the true extent of the 'lake district': with the largest sea Kraken Mare covering an estimated area of ~200,000 km2, approaching the size of Earth's Caspian Sea [Fig. 6]. The second largest sea, Ligeia Mare, has recently been named the target of a proposed future lake-lander mission, called TiME (short for Titan Mare Explorer).

So at last scientists had determined the extent of surface liquids: lakes and seas of hydrocarbons prevailed on Titan, rather than vast oceans. But the way of science is that each new advance in knowledge brings further questions, and this puzzle was no different. As Cassini enters its solstice mission phase we are left to wonder: how long ago were the floods that created the equatorial drainages? Why the asymmetry in lake coverage between north and south? Theories are already being advanced (e.g. Aharonson et al. 2009) but much work remains to be done before these lingering uncertainties are laid to rest.

2.2 Volcanoes or fissures?

The question of Titan's degree of liquid covering at least was quickly answered by Cassini. A related topic however has proved much more thorny, and no conclusion has yet been reached. The issue concerns Titan's atmospheric methane, and specifically whether the atmosphere is resupplied with this hydrocarbon from the interior, by means of volcanism, tectonic fissuring or other process.

The problem arises due to the continual destruction of methane in Titan's upper atmosphere, by action of sunlight (solar ultraviolet photons) and charged particle impacts originating from Saturn's magnetosphere. These processes are efficient enough that Titan's entire atmospheric methane inventory would vanish in a few tens of millions of years (Yung et al. 1984) - with far-reaching consequences including a decreased greenhouse effect and possible condensation out onto the surface of the entire remaining atmosphere (Lorenz et al. 1997)- unless the methane is somehow being replenished.

The long-serving paradigm has been that methane resupply must be an ongoing process, either continuous or at least episodic. Methane could plausibly have been captured during Titan's formation, and trapped in icy water-molecule cages called clathrates. Later, the primordial mixture of rock and ice would be warmed by natural radioactivity and begin to differentiate, with the rock sinking to form a solid core, while a molten mantle of ammonia-water antifreeze could develop above, capped by an icy crust. Periodic or ongoing destabilizations in the core and crust would result in convection, and perhaps eruptions of cryolava - icy slurry - would bring fresh methane to the surface. Expectations were therefore high that when Cassini finally imaged Titan closely no shortage of volcanic flows would be found.

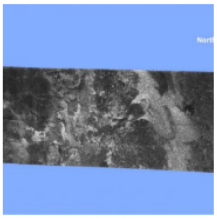
Figure 7

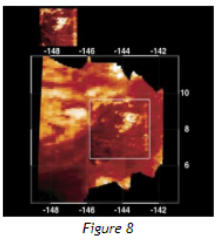

Figure 8

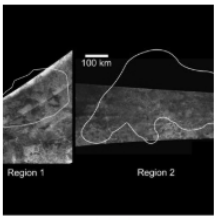

Figure 9

The initial reports were indeed encouraging. During the first close-up flyby of Titan on October 26th 2004, the Cassini SAR swept across a large, circular feature that was radar-dark, often indicating smooth terrain [Fig. 7]. The geologists on the team thought they recognized a similarity to volcanic structures on another world: the flattened 'pancake domes' of Venus (Lopes et al. 2007). The feature, named Ganesa Macula at 180 km across was much larger than the Venusian domes (10-30 km) and the height was later estimated at 2-5 km. During the same initial flyby, the VIMS team (Visible and Infrared Mapping Spectrometer) believed that had also struck cold 'gold'. They had spied a curious fan-like structure, apparently consisting of layered flows and initially dubbed 'the snail,' later given the more dignified title of Tortola Facula (Sotin et al. 2005) [Fig. 8].

These early enthusiasms were to prove unfounded, and illustrate the need for extreme caution in interpreting two-dimensional images as three-dimensional objects. The end for Ganesa came in 2008 at a meeting of the American Geophysical Society, when Randy Kirk of the Cassini Radar Team unveiled the results of a detailed topographical survey of 2% of Titan's surface. This was achieved by stereogrammetry - using the parallax information contained in two views of the same region from different directions. Ganesa was not a dome: the eastern edge is a mountain ridge - a topographical high - while the western side is a topographical low, and the compelling circular Ganesa feature itself is no more than a trick of the eye trying to impose order on disorder. The myth of Tortola Facula was similarly exploded by the merciless arc of the radar beams: it appeared as an unremarkable expanse of varied terrain with none of the apparent smooth lobes seen by the lower resolution of VIMS.

Yet, the idea of cryovolcanism continues to be compelling, if controversial. The latest salvo in the lava-wars has focused on the areas of Hotei and Tui Regios, where apparent lobate flows seen by radar were interpreted as cryovolcanic in origin (Wall et al. 2009) [Fig. 9], and photometric variability in VIMS near-infrared images was interpreted as ammonia frost in one area (Nelson et al. 2009a) and resurfacing in another (Nelson et al. 2009b). However the variability in at least the first area (Hotei) has been disputed by a later study (Soderblom et al. 2009).

What conclusions can we draw from this debate? Firstly, that interpreting the coarse images obtained through Titan's haze, and even

radar maps of Titan surface must be embarked on with extreme caution, preferably armed with knowledge of the topographical dimension from SAR stereogrammetry. Secondly, that Titan's surface is complex, with many processes responsible for its present-day morphology including aeolian, fluvial, tectonic, cryovolcanic and impacts. Regarding cryovolcanism, a consensus seems to have been reached that some flows are indeed volcanic, while others are fluvial deposits: determining which is which is a process that will doubtless be ongoing for the remainder of the mission. Meanwhile, the dream of seeing an unambiguously active volcanic outburst persists.

3. Conclusions

This article has aimed to introduce the reader to the vexing enigmas of Saturn's largest satellite - a world large enough to make a respectable planet, were it to orbit the Sun rather than Saturn. Titan was deemed important enough to deflect Voyager 1 from a course that could have taken it to an encounter with Pluto, instead to sail briefly past Titan for a tantalizing first encounter that answered too few questions (how big?) and left too many (what does the surface look like?)

Cassini in part, and especially Huygens were devised to answer Voyager's legacy of this world, especially concerning the nature of surface, and the connection of the interior, surface and atmosphere. In this regard, Cassini-Huygens has returned a wealth of results, but many of these have served merely to deep the mysteries so far. One topic that has attracted considerable attention is the idea of primitive life existing in the predicted interior ocean (Raulin 2008), or even on the surface using acetylene (C_2H_2) as a metabolic energy source (Oremland and Voytek, 2008).

Cassini now stands at its mid-point, and has seven more years (mechanical parts permitting) to study this enigmatic world. Many new discoveries will undoubtedly flow in this time, yet when the spacecraft finally departs Titan to plunge boldly into Saturn's clouds and a swift demise, there are sure to be as many remaining questions as answers. The case for a successor mission - or missions - is already building.

'May you live in interesting times' - so goes the apocryphal Chinese curse. But for those of us studying Titan with the powerful instruments on Cassini-Huygens, the undoubted 'interesting times' on this roller-coaster science mission seem fortunate indeed.

4. References

Aharonson O., Hayes A. G., Lunine J. I., Lorenz R. D., Allison M. D., Elachi C. (2009) An asymmetric distribution of lakes on Titan as a possible consequence of orbital forcing. Nature Geosciences 2:851-854.

Campbell D. B., Black G. J., Carter L. M., Ostro S. J. (2003) Radar evidence for liquid surfaces on Titan. Science 302:431-434.
Comas Sola, J., (1908). J. Br. Astron. Assoc. 19:151.

Combes M., Vapillon L., Gendron E., Coustenis A., Lai O., Wittemberg R., Sirdey R. (1997) Spatially Resolved Images of Titan by Means of Adaptive Optics. Icarus 129:482-497.

Coustenis A., Gendron E., Lai O., Veran J.-P., Woillez J., Combes M., Vapillon L., Fusco Th., Mugnier L., Rannou P. (2001) Images of Titan at 1.3 and 1.6 μm with Adaptive Optics at the CFHT.

Flasar F. M. (1983) Oceans on Titan? Science 221:55-57.

Kuiper, G. P., (1944) Titan: A Satellite with an Atmosphere. Astrophys. J. 100:378-

Lindal G. F., Wood G. E., Hotz H. B., Sweetnam D. N., Eshleman V. R., Tyler G. L. (1983) The Atmosphere of Titan: An Analysis of the Voyager 1 Radio Occultation Measurements. Icarus 53:348-363.

Lopes R. M. C., Mitchell K. L., Stofan E. R., Lunine J. I., Lorenz R., Paganelli F., Kirk R. L., Wood C. A., Wall S. D., Robshaw L. E., Fortes A. D., Neish C. D., Radebaugh J., Reffet E., Ostro S. J., Elachi C., Allison M. D., Anderson Y., Boehmer R., Boubin G., Callahan P., Encrenaz P., Flamini E., Francescetti G., Gim Y., Hamilton G., Hensley S., Janssen M. A., Johnson W. T. K., Kelleher K., Muhleman D. O., Ori G., Orosei R., Picardi G., Posa F., Roth L. E., Seu R., Shaffer S., Soderblom L. A., Stiles B., Vetrella S., West R. D., Wye L., Zebker H. A. (2007) Cryovolcanic features on Titan's surface as revealed by the Cassini Titan Radar Mapper. Icarus 186:395-412.

Lorenz R. D., McKay C. P. and Lunine J. I. (1997) Photochemically driven collapse of Titan's atmosphere. Science 275:642-644.

Lunine J. I., Stevenson D. J. and Yung Y. L. (1983) Ethane ocean on Titan. Science 222:1229-1230.

Meier R., Smith B. A., Owen T. C., Terrile R. J. (2000) The Surface of Titan from NICMOS Observations with the Hubble Space Telescope. Icarus 145:462-473.

Muhleman D. O., Grossman A. W., Butler B. J., Slade M. A. (1990) Radar Reflectivity of Titan. Science 248:975-980.

Nelson R. M., Kamp L. W., Matson D. L., Irwin P. G. J., Baines K. H., Boryta M. D., Leader F. E., Jaumann R., Smythe W. D., Sotin C., Clark R. N., Cruikshank D. P., Drossart P., Pearl J. C., Hapke B. W., Lunine J. I., Combes M., Bellucci G., Bibring J.-P., Capaccioni F., Cerroni P., Coradini A., Formisano V., Filacchione G., Langevin R. Y., McCord T. B., Mennella V., Nicholson P. D., Sicardy B. (2009a) Saturn's Titan: Surface change, ammonia and implications for atmospheric and tectonic activity. Icarus 199:429-441.

Nelson R. M., Kamp L. W., Lopes R. M. C., Matson D. L., Kirk R. L., Hapke B. W., Wall S. D., Boryta M. D., Leader F. E., Smythe W. D., Mitchell K. L., Baines K. H., Jaumann R., Sotin C., Clark R. N., Cruikshank D. P., Drossart P., Lunine J. I., Combes M., Bellucci G., Bibring J.-P., Capaccioni F., Cerroni P., Coradini A., Formisano V., Filacchione G., Langevin Y., McCord T. B., Menella V., Nicholson P. D., Sicardy B., Irwin P. G. J., Pearl J. C. (2009b) Photometric changes on Saturn's Titan: Evidence for cryovolcanism. Geophys. Res. Lett. 36:L04202.

Oremland R. S. and Voytek M. A. (2008) Acetylene as fast food: implications for development of life on anoxic primordial Earth and in the outer solar system. Astrobiology 8:45-58.

Raulin F. (2008) Astrobiology and habitability of Titan. Space Science Reviews 135:37-48.

Sagan C. and Dermott S. (1982) The tide in the seas of Titan. Nature 300:731-733.

Smith P. H., Lemmon M. T., Lorenz R. D., Sromovsky L. A., Caldwell J. J., Alison M. D. (1996) Titan's surface, revealed by HST imaging. Icarus 119:336-349.

Soderblom L. A., Brown R. H., Soderblom J. M., Barnes J. W., Kirk R. L., Sotin C., Jaumann R., Mackinnon D. J., Mackowski D. W., Baines K. H., Buratti B. J., Clark R. N., Nicholson P. D. (2009) The geology of Hotei Regio, Titan: Correlation of Cassini VIMS and RADAR. Icarus 204:610-618.

Sotin C., Jaumann R., Buratti B. J., Brown R. H., Clark R. N., Soderblom L. A., Baines K. H., Bellucci G., Bibring J.-P., Capaccione F., Cerroni P., Combes M., Coradini A., Cruikshank D. P., Drossart P., Formisano V., Langevin Y., Matson D. L., McCord T. B., Nelson R. M., Nicholson P. D., Sicardy B., LeMouelic S., Rodriguez S., Stephan K., Scholz C. K. (2005) Release of volatiles from a possible cryovolcano from near-infrared imaging of Titan. Nature 435:786-789.

Stofan E. R., Elachi C., Lunine J. I., Lorenz R. D., Stiles B., Mitchell K. L., Ostro S., Soderblom L., Wood C., Zebker H., Wall S., Janssen M., Kirk R., Lopes R., Paganelli F., Radebaugh J., Wye L., Anderson Y.,

Allison M., Boehmer R., Callahan P., Encrenaz P., Flamini E., Francescetti G., Gim Y., Hamilton G., Hensley S., Johnson W. T. K., Kelleher K., Muhleman D., Paillou P., Picardi G., Posa F., Roth L., Seu R., Shaffer S., Vetrella S., West R. (2007) The lakes of Titan. Nature 445:61-64.

Wall S. D., Lopes R. M., Stofan E. R., Wood C. A., Radebaugh J. L., Hörst S. M., Stiles B. W., Nelson R. M., Kamp L. W., Janssen M. A., Lorenz R. D., Lunine J. I., Farr T. G., Mitri G., Paillou P., Paganelli F., Mitchell K. L. (2009) Cassini RADAR images at Hotei Arcus and western Xanadu, Titan: Evidence for geologically recent cryovolcanic activity. Geophys. Res. Lett. 36:L04203.

Yung Y. L., Allen M. and Pinto J. P. (1984) Photochemistry of the atmosphere of Titan: Comparison between model and observations. Astrophys. J. Supp. 55:465-506.

5. Figure Captions

Figure 1. Artist's impression of the Huygens probe separating from the Cassini spacecraft on December 25th 2004, above the hazy atmosphere of Titan. (Image credit: NASA/JPL/Caltech).

Figure 2. Schematic view of Titan's atmosphere. (Credit: ESA).

Figure 3. Titan's surface imaged in 1994 by Smith et al. (1996), using the recently upgraded Hubble Space Telescope: Wide Field/Planetary Camera 2 (WFPC2). The four views are spherical projections based on 14 images taken at near-infrared wavelengths (from 0.85 to 1.05 microns) where Titan's atmosphere is semi-transparent: upper left - Saturn-facing hemisphere; upper right - leading hemisphere; lower left anti-Saturn hemisphere; lower right - trailing hemisphere. (Image Credit: UA Lunar and Planetary Laboratory; STScI.)

Figure 4. Images captured by the Descent Imager Spectral Radiometer (DISR) on Huygens, January 14th 2005. Upper left: from altitude 16.2 km, looking down on an apparent channel network draining to a shoreline at the edge of a dark plain. Lower left: view from altitude 8 km. Right: view from the surface. Rounded ice-cobbles are visible - the center cobble is about 4 cm across. (Image credit: ESA/NASA/University of Arizona.)

Figure 5. Cassini's first clear view of a lake: Ontario Lacus (black footprint shape) near Titan's south pole (marked by red cross) snapped by the Imaging Science Subsystem (ISS) on June 6th 2005 from a range of 450,000 km. (Image credit: NASA/JPL/Space Science Institute.)

Figure 6. Cassini Radar composite map of Titan's northern hemisphere from multiple SAR swaths, shown in false color to indicate presumed land (brown) and lakes (blue/black). Latitude circles are at 60, 70 and 80 degrees. The largest completely mapped lake (upper right) is Ligeia Mare, with an area of ~100,00 km^2. Kraken Mare (lower right) is only partly mapped, and may be twice as large. (Image credit: NASA/JPL/USGS.)

Figure 7. Radar SAR swath of Titan from first close Titan flyby of Cassini, October 26th 2004. Smoother terrain is darker (less backscatter towards receiver) whilst bright terrain is generally rougher. The large dark circle at the left end of the swath was a putative pancake dome of cryolava, named Ganesa Macula, at 50°N, 87°W. (Credit: NASA/JPL.)

Figure 8. The first suspected cryovolcano on Titan: Tortola Facula captured by Cassini's Visible and Infrared Mapping Spectrometer (VIMS), October 26th 2004. (Credit: NASA/JPL/University of Arizona.)

Figure 9. Cassini Radar images of two regions on Titan thought to show evidence for cryovolcanic flows. Region 1 is north of Hotei Arcus, about 400 km across and centered on 28°S, 78°W. Region 2 is western Xanadu at 7°S, 135°W and 900 km across.(Image credit: NASA/JPL.)

Book Review: Soil Carbon Dynamics

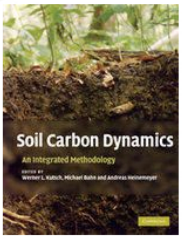

Soil Carbon Dynamics Cover

A Review of *Soil Carbon Dynamics, An Integrated Methodology* edited by W.L. Kutsch, M. Bahn and A. Heinemeyer (Cambridge University Press 2009)

Reviewed by Rattan Lal

This book describes methods to assess a vital natural resource: soil organic carbon (SOC) in natural and managed ecosystems. More than a billion people depend on the SOC pool to sustain their food supplies. Even so, certain areas have excess SOC that might help buffer and mitigate abrupt climate change. The significance of this book is heightened by its relevance to biodiversity, economic development, energy use, pollution abatement, and water quality.

The top meter of soil contains about 2500 gigatons (Gt) of SOC, roughly four times the biotic pool (620 Gt) and three times the atmospheric pool (800 Gt). Soil organic carbon is an important component of the global carbon cycle because it is a source and sink of trace gases and it moderates C-bearing atmospheric species. Concentrations of SOC vary in response to natural processes, but its recent and rapid variability results from agricultural management to optimize the soil nutrient pool and crop/biomass yields. Keep in mind that many details of how agriculture affects SOC are incompletely understood.

The SOC pool has been mined for plant nutrients since the dawn of settled agriculture some 10 to 13 millennia ago. Mineralization of soil organic matter, which contains about 58% SOC, releases Cu K, N, P, and Zn ions to soil water. These constituents are essential trace nutrients for corn, soybeans, wheat, and other crops. However, mineralization also emits CO_2 under aerobic and CH4 under anaerobic conditions. Agriculture often entails one or more of the following: biomass burning; deforestation; drainage and subsequent disruption of natural surface- and ground-water flow patterns; fertilization; tillage; and manure spreading. Each activity can contribute greenhouse gases to the atmosphere.

1. The global SOC pool has been depleted by 60 to 100 Gt, and most agricultural soils now contain less SOC than their maximum capacity. Soils that contain 10-40 megatons SOC/hectare may capture and immobilize excess CO_2 and other gases emitted by corporate and private farms, coal-burning power plants, petroleum processing, and other industries. Certain technological difficulties must be solved before large-scale CO_2 storage by SOC becomes an acceptable method to ameliorate greenhouse gas emissions. At present, CO_2 sequestration by SOC is hobbled by a lack of standard methodologies to measure and monitor its performance and to determine its cost-effectiveness. These issues are tractable engineering problems. Nevertheless, the idea is not accepted or even prioritized by the international community, including the very influential United Nations Framework Convention on Climate Change. (See COP-3 in Kyoto, December 1997 and COP-15 in Copenhagen, December 2009.)

The book edited by Kutsch et al. (2009) makes progress toward the goal of CO_2 sequestration by SOC. The book describes several techniques to accomplish the following: measure the magnitude of the SOC pool and its change over periods of 1 to 3 years: measure the impact of root respiration on SOC; characterize litter decomposition; account for microbial mediation of SOC; and develop models that compartmentalize total SOC according to how it formed. In this context, the book is a state-of-the-knowledge compendium of methods to monitor SOC pools and fluxes and its potential role in mitigating greenhouse gas emissions.

Statements and conclusions in the 15-chapter book are supported by comprehensive literature citations and illustrated by excellent graphics and flow charts. The book is prepared by world class-professionals and addresses an important and timely theme of global significance. This multi-authored collection should be read by participants in the U.N. Millennium Development Goal, which seeks to alleviate poverty and reduce malnutrition. The book describes essential techniques for trading C credits, which creates another income stream for farmers.

Readers will find this book extremely informative about chemical, ecological, physical and physiological aspects of soils. In addition, the chapter on the Kyoto Protocol reveals matters of interest for policy makers and practitioners. However, I find the book deficient in its discussion of soil quality and the human dimensions of C sequestration in soil. The book would benefit from four more chapters. The additional material should include:

1. The importance of the SOC pool in relation to agronomic production and global food security;
2. The cost-effectiveness and economics of C sequestration in soil compared to storage in geological formations;
3. How farmers and land managers ought to be compensated for devoting their land to enhancement of the SOC pool, and
4. Strategies to promote recommended management practices that would enhance the SOC pool in ecosystems affected by intensive agriculture.

About the Author

Rattan Lal is Professor of Soil Science and Director of Carbon Management and Sequestration Center at the Ohio State University, in Columbus, OH. He has authored, reviewed and edited 1,200 journal articles and publications during his career, and has published in a variety of journals including *Science* and *Soil & Tillage Research*. (lal.1@osu.edu)

Book Review: Protoplanetary Dust

Book Review of *Protoplanetary Dust: Astrophysical and Cosmochemical Perspectives*, Daniel Apai and Dante S. Lauretta, editors (2010) Cambridge University Press, New York, 377 pp., $120.

Reviewed by Harry Y. McSween

About 1% of the mass of interstellar matter in the Universe is dust. Most of the refractory elements are locked up in these tiny motes, leading to a depletion of those elements in the gas phase. This dust is a critically important component in the formation of stars and of planets. Dust cocoons around fledgling stars can be studied telescopically by their absorption and scattering of light. Laboratory simulations can provide constraints on the astrophysical processes that produce and alter dust in space. Dust that was incorporated into our own solar nebula and survived intact can be extracted from meteorites or collected by spacecraft and analyzed by sensitive instruments. The approaches provided by astronomical observations, laboratory experiments, and cosmochemical analyses are complementary. However, the practitioners of these disciplines seldom communicate with each other - and never more effectively than now.

Protoplanetary Dust comprises ten chapters by pairs or threesomes of authors from the different disciplines, each focused on the same question. These arranged marriages are intended to reveal new insights into the origin and evolution of dust in the Universe, and they succeed wonderfully. I found this novel approach riveting.

An instructive example of the complementary nature of the different approaches is provided by a chapter on dust particle size evolution. Astronomy is limited by the high optical depths in the inner parts of accretion disks, which preclude direct observation of the planet-forming regions. Conversely, meteorites only sample materials from the inner parts of our solar disk. Observations from astronomy and cosmochemistry can be combined with experimental data on dust coagulation to enhance understanding of how and where dust particles accrete to form planetesimals and ultimately planets.

Perhaps the most fascinating demonstration of the success of this book is illustrated by a figure that correlates the exquisite chronology of the early solar system afforded by short-lived radioisotopes in meteorites with the timescales of protostars, disks, and extrasolar planets estimated from astronomical observations. Anchoring these two very different evolutionary reference frames is a huge step forward.

The chapters cover a wide range of topics dealing with the origin, composition, physical state, and evolution of protoplanetary dust. Of particular interest to geochemists are Chapter 4 (Chemical and isotopic evolution of the solar nebula and protoplanetary disks), Chapter 5 (Laboratory studies of simple dust analogs in astrophysical environments), and Chapter 6 (Dust composition in protoplanetary disks).

The book is a marvel of coherency, and the editors have done a commendable job of ensuring that the same style and level of writing are maintained throughout. The intended audience is very broad, and although a few examples of astronomical or cosmochemical jargon creep in, such terms are defined in an excellent glossary. A few chapters end by identifying directions for future research - it would have been helpful to students if all of the authors had shared their own key questions. Helpful appendices provide background on mineralogy, mass spectrometry (why only this analytical technique?), and light absorption and scattering.

My only critique of this wonderful book is in its uneven treatment of condensation. This process (or sometimes the reverse process of evaporation) is commonly invoked to explain fractionations of refractory and volatile elements in solar system solids. Many chapters accept without question that condensation is the explanation for the isotopic homogeneity of nebular materials, but one states that 'To date, there is no incontrovertible evidence for direct condensation of rocky meteoritic material in the solar nebula.' It is not surprising that the authors of this book do not reach consensus on this on-going controversy. However, condensation is of such overriding importance in understanding protoplanetary dust that I wish the subject had been fully developed in its own chapter.

Protoplanetary Dust is a terrific edition (No. 12) to the Cambridge Planetary Science Series. The authors are authorities in their respective fields, and the interdisciplinary perspective crafted by the editors is a delight. This book should be required reading for all cosmochemists (and astronomers), and it would serve as an excellent text for an interesting graduate course on the origin of solar systems.

Book Review: On Fact or Fraud

A Review of *On Fact or Fraud: Cautionary tales from the front lines of science* by David Goodstein (Princeton University Press 2010)

Review By Eugenie Samuel Reich

The sociologist of science, Steven Shapin, once told me that he could not see the interest of studying fraud in science. Fraud, according to Shapin, revealed more about pathology of a few solitary individuals than anything about science as a whole. I've always felt instinctively that Shapin was wrong about this, and wished that he and other sociologists of science had spent more time understanding fraud. As a result, I was very happy to find a book that starts out from the same assumption that I have: that cases of fraud in science - including alleged, suspected and actual cases - can reveal something about the way science works. *On Fact and Fraud: cautionary tales from the front lines of science* is an accessible, well-written contribution to a relatively understudied area. It's by David Goodstein, whose background as a working physicist and administrator at the California Institute of Technology places him far from the sociology of science. Goodstein's book also contains some of the ingredients needed to prove Shapin wrong in his view of fraud, although I found that it stopped disappointingly short of reaching the conclusions that the ideas in it point towards.

Goodstein starts out by presenting a kind of back-of-the-envelope theory of fraud in science. According to Goodstein, fraudsters:

1. are under career pressure
2. think they know the answer their experiments will give and so do not bother to do the experiments properly
3. are working in a field where results are hard to replicate

The theory is a good start; the problem is that it doesn't go far enough. As Goodstein himself says, almost all scientists are under career pressure. Many scientists also think they know what their experiments will show. And science is also often hard to replicate. Why, then, do some scientists act fraudulently while others do not? Come to that, why do some frauds escalate into sensations that prove particularly embarrassing to the scientific community (the case of stem cell researcher Woo Suk Hwang of South Korea is a good example) while others are nipped in the bud early, for example, by a vigilant supervisor, trainee or colleague of the fraudster?

Goodstein's book falls short of answering these crucial questions. His theory on fraud is supplemented by some ideas about the social structure of science, which is described as containing a 'reward system' and an 'authority structure.' The 'reward system' covers all the ways that scientists express esteem for one another. The 'authority structure' guides and controls the reward system and includes the institutions in which scientists are employed (Goodstein mostly considers universities, but presumably this could include government and corporate laboratories as well). As scientists strive to work their way upwards in the 'reward system', scientific fraud is described by Goodstein as a temptation 'lurking quietly in the shadows', although never as something central to science. If this is granted, it becomes unclear how the ideas that Goodstein is presenting have helped to explain fraud. The problem is that Goodstein seems too reluctant to admit that fraud could be directly encouraged or magnified by features of the 'reward system' and 'authority structure.'

Further details, on the role played by the 'reward system' in fraud cases of the past, might have helped this account. For example, many scientists I have spoken to, especially junior ones still moving up the career ladder, complain about excessive pressure and rewards for getting into prestigious journals - notably *Nature* and *Science* -- which have tended to publish short accessible papers reporting on the latest results instead of long technical papers on experimental methods. Papers in such journals impress colleagues, and count heavily in a candidate's favor in tenure review procedures at universities, so they are undoubtedly an important part of today's 'reward system.' Yet cases of fraud in recent years have also made clear that the incentives to publish in these journals can act to the detriment of the truth. The physicist Jan Hendrik Schon was a post-doc and later staff scientist at Bell Labs in New Jersey at a time when submissions to *Nature* and *Science* were prized by managers. Schon became obsessed with the two journals and published eight papers in *Nature* and *Science* in 2001 -a young scientist at a top university would usually be lucky to publish two in a year. As I report in my book on Schon's case, when Schon was asked to write a long technical paper emphasizing methods rather than results, he even needed advice from a colleague about what other journal he might publish in!

Incentives operated similarly for the cloning scientist Woo Suk Hwang, who was prominent in South Korea at a time when the country was keen to improve the profile of its scientists internationally. Hwang took extreme steps to get two papers into *Science*, including fabricating the details of ethical protocols on the donation of human eggs, adding a figure of questionable data to a manuscript in response to questions from editors, and recruiting a respected American stem cell scientist, Gerald Schatten of the University of Pittsburgh, to co-author the work. Looking at such examples, as well at some of the breakthroughs that have lead to Nobel prizes (the painstaking work on blood antigens that lead to the discovery of hepatitis B by Baruch Blumberg is a good counterexample) one is driven to the conclusion that the scientific system works best when scientists place their emphasis on methodological and technical details that are the nuts and bolts of scientific breakthroughs. A change in science that rewarded solid methods instead of sexy results would make life harder for data-fabricators who tend to lack information on plausible methods because they have not really done the work.

Part of Goodstein's approach is to compare examples of fraud with examples of 'irreproachable' science. His main example of the latter is the discovery of high-temperature superconductivity in 1986. The period that followed the discovery of high-temperature superconductivity is famous for having involved lots of hyped and excessively enthusiastic claims. When I was reporting on Schon's case, I was regaled by tales of corner-cutting and ethical breaches in this area of physics. Goodstein does not consider any possible link between major frauds and an environment of hype. Yet Schon, whose case he does discuss, produced some of his more remarkable breakthroughs in the field of nanotechnology. Woo Suk Hwang was working in stem cells, also a field contaminated by hype at the time. Following Goodstein's theory we would gather that high-temperature superconductivity avoided a fraud scandal in part because the effect was easy to reproduce, and in part because it was a surprising phenomenon so that no one could have expected the results to come out the way they did. But this does not make the science of high-Tc 'irreproachable,' to use Goodstein's term. In fact ethical breaches did occur - one scientist told me that during high-Tc he learned about an important experiment by being asked to review a paper about it and immediately directed his own laboratory to study the same effect, hoping to get his own paper out on a competitive timescale. This scientist didn't see the problem with using the review process as a source of tip-offs when a field was very competitive.

About the Author

Eugenie Samuel Reich is a freelance science reporter in Cambridge, Massachusetts. She was a Knight Science Journalism Fellow at MIT for the academic year 2009/2010. She is the author of *Plastic Fantastic: How the Biggest Fraud in Physics Shook the Scientific World*.

Why then, does Goodstein steer so far clear of finding any fault with the scientific system. The reason, I strongly suspect, is that he is part of science himself, and wishes to avoid harming it by being too candid. Goodstein made his name as an authority on scientific misconduct while serving as vice-provost at the California Institute of Technology. He thanks the provosts at Caltech that he served under in the acknowledgment section of his book. His career at Caltech traced the emergence of a unified federal policy on research misconduct, including controversies such as the notorious Baltimore case, when Nobel Laureate David Baltimore defended a collaborator against accusations of misconduct at MIT. Baltimore went on to become president of Caltech, including at the time that Goodstein was vice-provost. Goodstein is up front about all of these connections, but in several places allows the bias that arises from it to influence his accounts without apparently realizing he is doing so. For example, he discusses two cases of fraud in biology at Caltech that he says were handled in an exemplary fashion, but omits to discuss the case of Luk Van Parijs, an associate professor of immunology at MIT who in 2007 was found guilty of misconduct committed at Caltech while working in Baltimore's lab, including on two papers on which Baltimore was the senior author (the research was retracted in 2009). Despite widespread rumors and credible allegations against Van Parijs' work at MIT, Caltech failed to investigate Van Parijs' work at their institute until irregularities were brought explicitly to Baltimore's attention by a journalist (myself, while working on an article about the case for *New Scientist* magazine). Another place Goodstein's bias interferes is in his account of Robert Millikan, a Caltech professor who won the Nobel prize for measuring the charge on the electron using oil droplets. Historian of science Gerald Holton published some pioneering historical work in 1978 showing that Millikan, despite claiming in one paper to be reporting on every drop he studied, in fact omitted to report on some of the droplets he had studied. Goodstein lapses into a troubling apologism for seriously unethical misbehavior when he writes that Millikan probably forgot about the omitted droplets.

Taken together Goodstein has generated a useful primary source that documents, in that it suffers from, some of the bias that senior people in today's scientific community have when it comes to dealing with fraud. The major problem that institutions are usually reluctant to investigate or to publicize their own failings - as with Caltech in the case of Van Parijs - is barely addressed in the book and ideas bearing on the motive for fraud are not filled out in detail. Parts of the book nevertheless make for a thoughtful contribution to the landscape of reading on fraud and select sections - such as the introduction - may be worth adding to the syllabi for ethics and misconduct courses.